Kinetic Isotope Effects for Adiabatic Proton Transfer Reactions in a Polar Environment

Philip M. Kiefer[†] **and James T. Hynes***[,†,‡]

Department of Chemistry and Biochemistry, University of Colorado, Boulder, Colorado 80309-0215, and Département de Chimie, CNRS UMR 8640 PASTEUR, Ecole Normale Supérieure, 24, rue Lhomond, 75231 Paris, France

Received: July 22, 2003

A nontraditional picture for primary kinetic isotope effects (KIEs) is presented for proton transfer (PT) reactions in a polar environment in the proton adiabatic regime, in which proton motion is quantum mechanical, but is not tunneling. The description differs from the "standard" treatment of KIEs for PT in both the quantization of the proton nuclear motion and the identification of a solvent coordinate as the reaction coordinate. KIEs resulting from a free energy relationship (FER) based on this adiabatic PT description recently derived (Kiefer, P. M.; Hynes, J. T. *J. Phys. Chem A* **2002**, *106*, 1834,1850) are presented. It is shown that key experimental consequences thought to validate the standard picture for KIEs *also* follow from this nontraditional picture, including those for (i) Arrhenius temperature behavior, (ii) dependence on reaction asymmetry ΔG_{RXN}, (iii) the magnitude of the KIE, and (iv) the Swain−Schaad relationship. A detailed comparison between the present picture and the standard description is presented.

1. Introduction

Proton transfer (PT) is of obvious importance in both chemistry and biology;[1] accordingly there has been intensive study of PT rates in solution and other polar environments, including proteins.[1−4] A widely used and valuable experimental technique to probe aspects of PT reactions is isotopic substitution and comparison of the rates of transfer of a proton, deuteron, and triton. Information from primary kinetic isotope effects (KIEs) for PT reactions has allowed interpretation of the rate-limiting step in complex reactions and provided insight into the microscopic nature of the transition state (TS).[1−5] In the present work, we present a theory of KIEs, which differs fundamentally from "standard" descriptions, for what we term *adiabatic* PT reactions, which as described within, are characterized by a nontunneling but still quantum behavior of the proton motion.

The standard view of the origin of KIEs traces back toWestheimer and Melander (W−M).[6] In its simplest version, this picture uses a linear three-center molecular system for PT, illustrated here for the case of an acid−base reaction within a hydrogen-bonded (H-bonded) complex:

$$AH\cdots B \rightarrow A^{-}\cdots HB^{+} \qquad (1.1)$$

(Actually, these descriptions, which focus on isolated molecule considerations, are more appropriate for H atom transfers than for PT. Because, however, similar ideas are used in connection with condensed phase PT, we include it here and draw attention to special additional features for PT, such as strong coupling to the solvent as well as reactant and product H-bond complex features.) The reaction potential surface is a function of two coordinates, the A−H proton distance and the distance between the two heavy moieties, A···B. Along the minimum energy path, the reaction begins at large heavy atom separation with the A−H proton distance constant, proceeds through a TS A···H···B and goes onto products with large A−B separation and constant H−B distance to produce $A^{-}\cdots HB^{+}$. Using TS theory, the KIE arises from the exponentiated activation energies.[1,5−7] For H versus D transfer, the KIE is given by

$$k_H/k_D \approx \exp[-(\Delta G_H^{\ddagger} - \Delta G_D^{\ddagger})/RT$$

$$\Delta G_H^{\ddagger} - \Delta G_D^{\ddagger} \approx ZPE_H^{\ddagger} - ZPE_H^{\ R} - ZPE_D^{\ddagger} + ZPE_D^{\ R} \qquad (1.2)$$

As is of course well-known, the KIEs originate, in this framework, from isotopic zero point energy (ZPE) differences between the reactant and TS.[1,5−8]

The relevant ZPE in the reactant region is just the ZPE of the A−H vibration in the reactant A−H···B complex, the motion transverse to the reaction coordinate in this region. For a thermodynamically symmetric reaction ($\Delta G_{RXN} = 0$), the reaction path through the TS consists solely of the proton's classical motion over the barrier, so that there is no proton ZPE associated with this motion at the TS. Rather, the TS ZPE is associated with the transverse motion at the TS (just as for the reactant), which in the collinear model is a symmetric stretch, the heavy particle A−B vibration.

For such a symmetric reaction, the reactant ZPE is larger for H than for D, $ZPE_H^R > ZPE_D^R$, due to the lower reactant AH stretch vibration frequency for the more massive D. At the TS, $ZPE_H^{\ddagger} = ZPE_D^{\ddagger}$, because the TS symmetric stretch motion does not involve the central L (L = H, D, or T) species. The result is the complete "loss" of the ZPE for the proton stretching mode on going from reactant to TS. Typical reactant proton stretch frequencies ($\omega_{CH} \sim 3000$ cm^{-1}) and a simple mass correlation between ZPEs (i.e., $ZPE_D \approx ZPE_H/\sqrt{2}$) give an H vs D KIE of about 7 at room temperature.[1,5−7]

It was appreciated, however, that the observed wide range in KIE magnitudes cannot be accounted for by the range in the reactant proton vibration frequencies, and in the W−M picture, this range is attributed, with eq 1.2 still applying, to the variation

* To whom correspondence should be sent. Phone: (303) 492-6926. Fax: (303) 492-5894. E-mail: hynes@spot.colorado.edu.
† University of Colorado.
‡ Ecole Normale Supérieure.

10.1021/jp030893s CCC: $25.00
Published on Web 09/30/2003

in the KIE with reaction asymmetry ΔG_{RXN}, as follows.[1,5−7] For an asymmetric reaction, the reaction coordinate at the TS includes both proton and heavy particle motions. Consistent with the Hammond postulate,[9] the TS becomes more geometrically similar to the product as the reaction becomes more endothermic, and more similar to the reactant as it becomes more exothermic. Thus the *transverse* vibration at the TS, whose ZPE is relevant for the rate, more and more involves the proton motion, and in either limit approaches the bound proton stretch vibration of the product BH or the reactant AH. This effect decreases the KIE, resulting in a k_H/k_D vs ΔG_{RXN} trend that is maximal at $\Delta G_{RXN} = 0$ and drops off as the reaction becomes more endo- or exothermic.

For PT, there are four common experimental observations that are consistent with the standard picture described above: (i) the Arrhenius temperature dependence of the KIE (as well as of the individual isotope rateconstants); (ii) the KIE − ΔG_{RXN} behavior described above; (iii) the KIE range of ∼2−10; (iv) the wide applicability of the Swain−Schaad relationship[7,10] connecting ratios of KIEs (e.g., $k_H/k_T = (k_D/k_T)^{3.3}$), which follows directly from eq 1.2 and its variants. In succeeding sections, we will argue that all four of the above observations also follow directly from a quite different picture of PT reactions in a polar environment.

We pause to note that the standard picture can be supplemented with a quantum contribution for classical motion over the barrier at the TS via a tunneling correction.[7,11,12] Various departures from the above four experimental observations, such as non-Arrhenius rate behavior or KIEs much in excess of 10, are typically taken as indicating tunneling.[1,4,5,7,12,13] Addition of tunneling corrections to the standard PT rate will obviously affect the KIE, including its reaction asymmetry dependence.[7,12] Indeed, it has been argued that variation of the tunneling contribution versus reaction asymmetry is primarily responsible for the broad range in magnitude of observed KIE versus reaction asymmetry plots, instead of the variation of ZPE at the TS described above.[12] Further discussion of this is reserved for a separate paper on KIEs for the *nonadiabatic*, proton tunneling regime.[14] We stress that in the present work we only consider PT systems in which the proton does *not* tunnel.

Despite the success of the standard picture described above, it is useful to point out why a different picture would be more plausible. First, the standard description has a certain logical inconsistency in the TS description. In the symmetric case, proton motion is viewed as completely classical over the proton barrier. For any finite reaction asymmetry, however, the quantum character of the proton as a bound quantum vibration becomes extremely important, because it is that character that influences the frequency, and thus the ZPE of the transverse TS motion. It seems difficult to maintain that proton motion within an H-bond can be both classical and quantum. In the theory described within, the proton motion is *always* treated as a quantum vibration with a given ZPE, for both symmetric and asymmetric reactions.

Further, the standard picture presented above makes no reference to the solvent. To the degree that the solvent is included in standard descriptions, it is imagined to alter the rate via a differential equilibrium solvation of the TS and the reactant, again all within the standard framework recounted above.[15,16] But the equilibrium solvation assumption, which requires, e.g., that the solvent motion is fast compared to the relevant motion of the reacting solutes in the TS region, is not at all plausible in the case of high-frequency quantum proton motion; indeed, the opposite situation is more appropriate: the solvent is generally slow compared to the proton motion.[19−24]

Our main line of analysis of KIE for adiabatic PT reactions exploits a major result of our previous work;[26] a nonlinear free energy relationship (FER) between the reaction activation free energy $\Delta G^{\ddagger}$ and the reaction asymmetry ΔG_{RXN} for adiabatic PT was derived, with molecular expressions given for its ingredients, utilizing a physical picture that differs considerably from the standard view. The PT reaction within an H-bonded complex in eq 1.1 is viewed as driven by configurational changes in the surrounding polar environment; the fast proton vibration adiabatically follows the environment's slower rearrangement, and one considers the instantaneous proton potential for different environmental arrangements.[27] The reaction activation free energy is largely determined by the reorganization of this environment, such that the reaction coordinate is a solvent coordinate, together with certain ZPE changes associated with the quantized proton motion. In contrast, traditional approaches would instead focus on the height of any potential barrier in the transferring proton's coordinate, and that coordinate is regarded as a component in the classical reaction coordinate, especially at the TS in the thermodynamically symmetric case, where it constitutes the entire reaction coordinate.[1,6,7,12,28] In the present adiabatic PT picture for such a symmetric reaction, at the TS in the solvent coordinate, the proton motion is instead a bound quantized vibration above the proton barrier; the proton motion is thus a transverse, rather than a reaction coordinate.[26]

As discussed in detail in ref 26, the adiabatic PT regime is expected to apply for proton donor/acceptor systems in which there is an H-bond of sufficient strength, such that when a symmetric proton potential is established, its barrier height is sufficiently low that the ground proton vibrational level is above it. (Even for the high proton barrier case, not discussed here, the adiabatic PT limit represents the "over the barrier" contribution to the rate, with further contributions arising from quantum tunneling.)

The underlying electronic structure in ref 26 was described by a superposition of the two limiting neutral (N) and ionic (I) structures for the two valence bond (VB) states with different charge character corresponding to that of the reactant and product in eq 1.1,

$$|\Psi\rangle = c_N|\Psi_N\rangle + c_I|\Psi_I\rangle \qquad (1.3)$$

along the lines of the Mulliken picture of PT reactions.[29] Strong electronic coupling (∼1 eV) between these VB states in the presence of the solvent produces the ground electronically adiabatic surface on which the reaction occurs. The evolving proton potential includes the differential (nonequilibrium) solvation by the surrounding environment.

The FER derived in ref 26 was shown to differ numerically in only a minor fashion from the empirical Marcus FER for PT,[28] despite a completely different physical picture for the two FERs. This result is important because experimental (H/D) KIE versus ΔG_{RXN} behavior is often modeled with a KIE expression derived from the Marcus FER.[2,5,7,28] We will compare and contrast the KIE predictions of the FER of ref 26 with that of Marcus in the section 4 discussion.

The KIE calculations in this paper presented to illustrate the concepts have all been performed using the same oxygen donor−oxygen acceptor H-bond model for acid−base PT within an H-bonded complex used to derive the FER,[26] except that of course the proton is sometimes changed to a deuteron or triton. Different reaction asymmetries were obtained from several

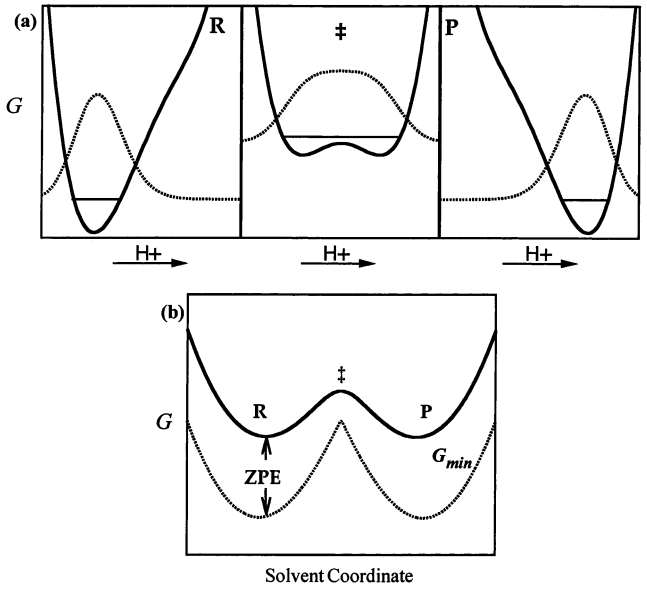

Figure 1. (a) Free energy curves versus proton position at the reactant R, transition state ‡, and product P solvent configurations for a symmetric reaction. In each case, the ground-state proton vibrational energy level (solid line) and wave function (dotted line) are indicated. (b) Free energy curve for the symmetric PT system displayed in (a) with the proton quantized in its vibrational ground state versus solvent reaction coordinate (solid line). The solvent coordinate critical points corresponding to the proton potentials in the upper panel are indicated. The free energy at the minimum of the proton potential along the solvent coordinate G_{min} (dotted line) is also shown.

values of gas-phase offsets between the two VB states in eq 1.3 for the H-bonded complex as described previously.[26]

The outline of the remainder of this paper is as follows. Section 2 briefly reviews the nonequilibrium solvation picture for adiabatic PT and the free energy $\Delta G^{\ddagger}$ versus ΔG_{RXN} relationship derived therefrom and analyzes the isotope dependence in the FER. Section 3 presents the resulting primary KIEs, demonstrating that the four experimental observations noted above, typically taken as support for the standard view, e.g., the KIE trend versus reaction asymmetry, follow naturally from the present theory. Section 4 presents a physical interpretation of the KIEs, including a comparison of our approach and predictions with others, i.e., that of the standard picture and that utilizing the Marcus FER. Concluding remarks are offered in section 5.

2. Isotope-Dependent Free Energy Relationship: $\Delta G^{\ddagger}$ vs ΔG_{RXN}

2a. General Picture. In the underlying picture of PT reactions[19−23,30] employed within, the reaction is driven by configurational changes in the surrounding polar environment, a feature of much modern work on PT reactions,[19−23,26,31] and the reaction activation free energy is largely determined by the environmental reorganization. In this adiabatic PT picture, the rapidly vibrating proton adiabatically follows the environment's slower rearrangement, thereby producing a perspective in terms of the instantaneous proton potential for different environmental arrangements. Here we briefly describe the overall picture, emphasizing isotopic-dependent aspects as a preliminary for the discussion of the free energy relationship and its isotope dependence in sections 2b and 2c.

Figure 1 displays the key features for a model overall symmetric PT reactionin a linear H-bonded complex. Figure 1a shows the proton potential curves versus the proton coordinate, for solvent configurations appropriate to that of the reactant pair, the TS, and the product pair. These different states of solvation, or more simply the solvent's electric nuclear polarization state, distort the potential from being initially asymmetric favoring the proton residing on the acid, through an intermediate situation where a proton symmetric double well is established, and on to an asymmetric potential now favoring the proton residing on the base. The solvent motion is critical, due to the strong coupling of the reacting pair's evolving charge distribution to the polar solvent. Finally, as a technical point, the solvent coordinate ΔE in this picture is an alter ego of the solvent polarization, related to a certain energy gap defined such that for a thermodynamically symmetric PT reaction, it has a value of zero at the solvent TS where the proton potential is symmetric.[32,33]

For each of the three proton potentials in Figure 1, the quantized ground vibrational energy, i.e., the ZPE, is indicated. For the TS solvent configuration, the zero point level is above the proton barrier, the hallmark of the quantum adiabatic PT limit. (This situation is to be contrasted with the case where the level is below the barrier top, such that the reaction would involve proton tunneling.[19,20,23,31]) Here the proton motion is a bound quantum vibration; there is *no* classical barrier crossing of the proton, in contrast to the standard description of conventional TS theory.[34] We draw special attention to the proton's very considerable quantum delocalization in the middle panel of Figure 1a, to be contrasted with a classical, localized proton description. This adiabatic PT regime picture has been supported in electronic structure calculations and simulation studies including acid ionizations in solution[21,22,35] and elsewhere.[21−23,36] The above-the-barrier proton zero point level at the reaction TS corresponds to what has been termed in the enzyme reaction literature a "low barrier H-bond"[37] situation.

In this adiabatic limit, the high-frequency quantum proton vibration adiabatically adjusts to the reorganizing solvent, the reaction coordinate is a solvent coordinate, rather than the proton coordinate, and there is a free energy change up to the TS activation free energy as the solvent rearranges, as shown in Figure 1b. This change involves a free energy cost associated with the solvent rearrangement and a change in the proton ZPE, now more fully discussed.

The total free energy of the reacting system versus the solvent reaction coordinate can be usefully decomposed into two basic contributions,[26,36] as shown in Figure 1b,

$$G = G_{min} + \mathrm{ZPE} \tag{2.1}$$

These are respectively, a "bare" free energy, G_{min}, corresponding to the situation where the proton is located at its *classical* minimum position for any given solvent coordinate value, and the vibrational ZPE of the proton, measured from the latter potential energy minimum. The ZPE decreases as the TS in the solvent coordinate is approached, because the proton potential is becoming more symmetric and the proton is delocalized in a larger potential region. Though both contributions to the overall free energy are cusped, due to the shift in the proton's minimum position as the symmetric proton potential situation is passed, the overall free energy profile is of course continuous.[26,36] The reaction asymmetry in Figure 1b is primarily determined by the asymmetry in G_{min}, mainly because the ZPE versus solvent coordinate behavior is independent of reaction asymmetry.[26] The decomposition in eq 2.1 will prove useful for analyzing KIEs because the isotope-dependent ZPE component of G is isolated from the isotope-independent *classical* free energy curve G_{min}.

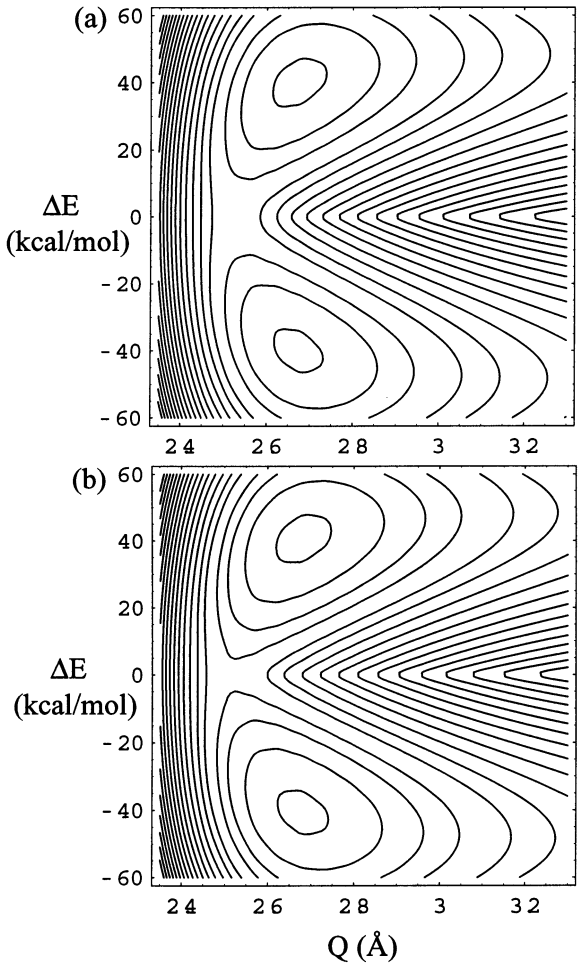

Figure 2. Contour plot of the PT system free energy $G(Q,\Delta E)$ with the proton (a) in its ground vibrational state versus the solvent coordinate, ΔE, and the AB separation, Q, for a symmetric reaction; (b) Same as in (a) except a deuteron replaces the proton. Contour spacings are 1 kcal/mol. The surfaces were generated with a model system, with the electronic structure described using the two VB states shown in eq 1.3.

The description in Figure 1 has ignored any bending contribution, an approximation justified for a linear H-bonded complex in the adiabatic limit in section 4. It has also ignored, for simplicity, the influence of the separation between the heavy donor and acceptor moieties between which the proton is transferred, i.e., the H-bond coordinate. This coordinate has been shown to be important in the adiabatic PT regime,[21−23,26,38] reflecting a significant coupling between the H-bond coordinate and the solvent coordinate.[26] We now briefly review this coupling, emphasizing the effect of isotopic substitution.

For this purpose, we display in Figure 2 calculated free energy surfaces for H and D transfer reactions for a symmetric ($\Delta G_{RXN} = 0$) oxygen donor−oxygen acceptor PT pair, versus the solvent coordinate ΔE and the H-bond coordinate Q. These surfaces have the proton or deuteron *already* quantized in its ground vibrational state,[26] such that the coordinate of either particle no longer appears.

Both surfaces contain two minima depicting the reactant and product complexes ($Q \sim 2.7$ Å). We define the *intrinsic* rate of PT (or DT) as the interconversion of these complexes (and thus, no diffusional rate of formation of these complexes is included). The floors of the valleys in the solvent coordinate are more narrowly separated as Q decreases on the way to the surface's saddle point. This saddle point, located at $\Delta E = 0$ and $Q \sim 2.5$ Å, would define a TS in the perspective that Q is classical. (Although the H-bond vibration will be quantized presently, a preliminary discussion in terms of a classical Q perspective proves useful.) From Figure 2, one can see that the barrier height going from either complex to the TS is larger for D than for H. As discussed in detail later in this section, the difference in barrier heights is primarily due to a smaller difference in ZPE between reactant and TS for D than for H. Figure 2 also shows the important feature that the H-bond force constant, and thus its frequency, varies with the solvent coordinate ΔE, increasing as the saddle point is reached from either the reactant or product.

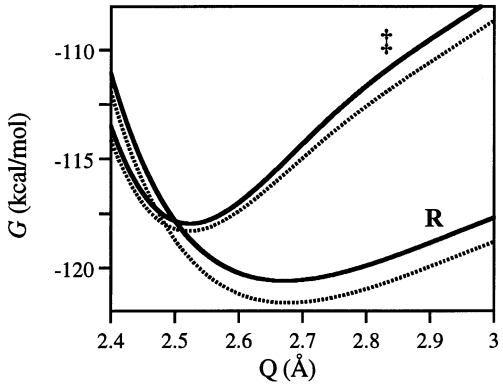

Figure 3. Cuts of the two-dimensional surfaces in Figure 2, at two different solvent coordinate values $\Delta E = -40$ kcal/mol (R) and $\Delta E = 0$ (‡). The solid lines are from the proton quantized surface, Figure 2a, and the dotted lines are from the deuteron quantized surface, Figure 2b.

This compression of the H-bond coordinate Q and increase in H-bond frequency from the reactant complex to the TS indicate a strong coupling between the H-bond coordinate features of the surface and the solvent coordinate. This is further highlighted by taking cuts in the surfaces in Figure 2, representative of the reactant, $\Delta E = -40$ kcal/mol, and the TS, $\Delta E = 0$ (see Figure 3). Both H and D curves show a similar compression in Q going from $Q \sim 2.7$ Å in the reactant to $Q \sim 2.5$ Å at the TS, with the equilibrium H-bond position slightly larger for D in both the reactant and the TS. The H-bond frequency change is also apparent in Figure 3, going from $\hbar\omega_Q = 290$ cm^{-1} for H and $\hbar\omega_Q = 285$ cm^{-1} for D in the reactant to a higher frequency at the TS, $\hbar\omega_Q = 550$ cm^{-1} for H and $\hbar\omega_Q = 540$ cm^{-1} for D. These features are consistent with the general expectation that H-bonds are stronger at smaller H-bond lengths[39] and with experimental measurements for the geometries of H-bond systems with different equilibrium symmetries.[40] The H-bond-solvent coordinate coupling responsible for these basic features is discussed in detail in ref 26, where it is shown that it primarily arises from the increased mixing of the electronic character of the reactant and product states as Q decreases (cf. eq 1.3); this mixing of the neutral and ionic wave functions in eq 1.3 is most important near the TS, and it is more sensitive to the H-bond separation there. The slight variations between H and D in the reactant and TS frequencies arise from the difference in variation of the ZPE with respect to the solvent and H-bond coordinates, with larger variation occurring for the lighter H, and will be discussed further in connection with FER coefficients in section 2b.

The H-bond vibrational mode frequency is typically sufficiently high, e.g., ∼550 cm^{-1} in the TS region for our model system, to require its quantization. In this description, constructed in ref 26b, both the H-bond *and* proton vibrational modes are quantized simultaneously for each solvent configuration, because the time scale of the solvent is often slower than

that of the H-bond vibration as well as the proton vibration. This results in a one-dimensional free energy curve similar to that in Figure 1b. The PT rate constant expression including the quantized H-bond vibration is the thermal average of the PT rate constant for each H-bond vibrational state i,[21c,26b] each having a TS theory form:[41]

$$k_i = (\omega_{Si}/2\pi)\exp(-\Delta G_i^{\ddagger}/RT) \qquad (2.2)$$

Here ω_{Si} is the reactant region solvent reaction coordinate frequency, and $\Delta G_i^{\ddagger}$ is the free energy barrier for PT for the ith H-bond vibrational state. The free energy barrier is the barrier in the solvent coordinate, which includes a difference in the ZPEs of the proton *and* the H-bond vibration between the reactant and the TS (See Figure 1b). Because the H-bond vibration frequency is $\sim$290 cm^{-1} in the reactant and product states and is larger at the TS ($\sim$550 cm^{-1}), the reaction barriers for excited H-bond vibrational states are larger than for the ground state $i = 0$.[26b] Consequently, the PT and DT rates are dominated by dynamics in the ground H-bond vibrational state,[26] and hereafter we deal only with the $i = 0$ case.[42]

Figure 4 displays the H and D free energy curves for a symmetric and an asymmetric reaction. Again, the total free energy G has a decomposition of the form in eq 2.1. The free energy G_{min} evaluated at the classical minima for both the proton and H-bond coordinates at a given solvent coordinate value is indicated as the lower curve in Figure 4a,b. The ZPE contributions for both H and D from Figure 4a,b are displayed as Figure 4c and contain both the ZPE of the H or D vibration and that of the H-bond mode. The reaction barrier increases starting from an exothermic case (Figure 4b) to an endothermic case (reverse of Figure 4b). From Figure 4a,b, one can note that both the reactant well frequency ω_s and barrier height $\Delta G^{\ddagger}$ are isotope-dependent. However, the contribution of ω_s to the KIE magnitude will be shown to be minimal in section 3, and we thus focus on the isotope dependence of the reaction barrier height variation with reaction symmetry.

One should also note from Figure 4a,b that the position of the TS along the solvent coordinate $\Delta E^{\ddagger}$ shifts with reaction asymmetry. Even though both G_{min} and ZPE are cusped at $\Delta E = 0$, G is continuous; the ZPE behavior softens the G_{min} discontinuity at $\Delta E = 0$. The addition of the ZPE to an asymmetric G_{min} (cf. Figure 4b) shifts the maximum of G away from the maximum of G_{min} at $\Delta E = 0$, in the direction consistent with the Hammond postulate,[9] e.g., later for endothermic reactions. It is important to remark that this indicates that the ZPE contribution at $\Delta E^{\ddagger}$ to the free energy barrier $\Delta G^{\ddagger}$ in the solvent coordinate will increase with increasing reaction asymmetry, a crucial qualitative characteristic.[26] Also visible in Figure 4b is the isotope dependence of the shift $\Delta E^{\ddagger}$ and the associated increase of ZPE at $\Delta E^{\ddagger}$ with increasing reaction asymmetry; the latter will lead to a reduction in the KIE, because the ZPE contribution at $\Delta E^{\ddagger}$ will become more and more similar to that of the reactant. The quantitative analysis of these features and their importance in KIEs will be discussed in section 2b.2, but from Figure 4, one can already see that the *variation* in ZPE along the reaction coordinate and its isotopic difference will play a significant role in the reaction free energy barrier variation, and hence the KIE as well.

2b. Free Energy Relationship. The $\Delta G^{\ddagger}$ vs ΔG_{RXN} FER derived for adiabatic PT in a polar environment (cf. eq 1.3 of ref 26b) is

$$\Delta G^{\ddagger} = \Delta G_o^{\ddagger} + \frac{1}{2}\Delta G_{RXN} + \frac{1}{2}\alpha_o'\Delta G_{RXN}^{\ 2} \qquad (2.3)$$

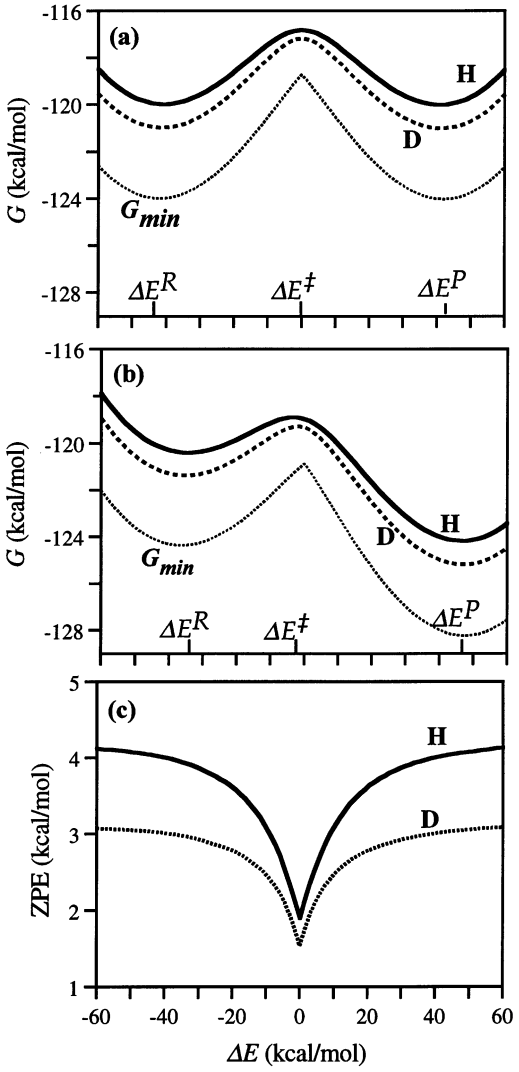

Figure 4. Ground-state free energy curves (solid lines H and dashed lines D) with both the proton/deuteron and H-bond vibrations quantized: (a) symmetric reaction and (b) exothermic reaction. Dotted lines show the free energy curves G_{min} excluding the ZPE. (c) The ZPE for the proton (solid line) and deuteron (dotted line), including H-bond vibration, vs ΔE. The dashed curves in (a) and (b) plus the ZPE in (c) give the full free energy G, the solid curves in (a) and (b). ΔE^R, ΔE^P, and $\Delta E^{\ddagger}$ denote the reactant, product, and TS solvent coordinate values, respectively.

where $\Delta G_o^{\ddagger}$ is the "intrinsic" reaction barrier $\Delta G_o^{\ddagger} = \Delta G^{\ddagger}(\Delta G_{RXN} = 0)$, and α_o' is the Brønsted coefficient slope evaluated at $\Delta G_{RXN} = 0$.[43] These quantities will be key in all that follows. The coefficient of the linear term is the Brønsted coefficient for the symmetric reaction, $\alpha_o = {}^1/_2$; this value reflects equal contributions of the VB electronic resonance structures representative of the reactant and product states to the electronic structure of the reacting pair at the symmetric reaction TS[26] (cf. eqs 1.1 and 1.3).

The intrinsic free energy barrier $\Delta G_o^{\ddagger}$ is composed of a contribution $\Delta G_{m,o}^{\ddagger}$ due to a certain solvent reorganization and the difference $Z_o^{\ddagger} - Z_o^{R} = \Delta ZPE_o^{\ddagger}$ in the ZPEs of the protonic and H-bond coordinates between the reactant and the TS for the symmetric reaction (cf. eq 1.4 of ref 26b)

$$\Delta G_o^{\ddagger} = \Delta G_{m,o}^{\ddagger} + \Delta ZPE_o^{\ddagger} \qquad (2.4)$$

The Brønsted coefficient

$$\alpha = \frac{\partial \Delta G^{\ddagger}}{\partial \Delta G_{RXN}} \tag{2.5}$$

is quantitatively described in the adiabatic PT picture both by the relative difference between the TS and the reactant of (a) the separation in the solvent coordinate and (b) the electronic structure via

$$\alpha = \frac{\Delta E^{\ddagger} - \Delta E^{R}}{\Delta E^{P} - \Delta E^{R}} = \frac{\langle c_I^2 \rangle^{\ddagger} - \langle c_I^2 \rangle^{R}}{\langle c_I^2 \rangle^{P} - \langle c_I^2 \rangle^{R}} \tag{2.6}$$

(see eq 5.39 in ref 26a; the same result applies when both proton and H-bond coordinates are quantized). Here $\Delta E^{\ddagger} - \Delta E^{R}$ is the reaction coordinate distance between the TS and reactant, and $\Delta E^{P} - \Delta E^{R}$ is the corresponding distance between the product and reactant. $\langle c_I^2 \rangle$ is the *quantum* average over the proton and H-bond vibrations of the limiting product ionic contribution to the electronic structure c_I^2 (see eqs 1.1 and 1.3). The electronic structure for each critical point $\langle c_I^2 \rangle^c$ (c = R, P, and ‡) is evaluated at the respective critical point position along the reaction coordinate ΔE^c ($\Delta E^c = \Delta E^R$, ΔE^P, or $\Delta E^{\ddagger}$). As noted above, the TS structure (and TS position along the reaction coordinate) for a symmetric reaction is halfway between that of the reactant and product, and $\alpha_o = {}^1/_2$, independent of isotope.

The Brønsted coefficient α has often been used to describe TS structure via the Hammond postulate[9] or the Evans−Polanyi relation,[44] where α is the relative TS structure along the reaction coordinate, usually a bond order or bond length. Although adiabatic PT has a quite different environmental coordinate as the reaction coordinate, eq 2.6 is consistent with that general picture. The first expression in eq 2.6 explicitly describes α in terms of the relative position of the TS along the reaction coordinate ΔE, and the second expresses this in terms of the values of the electronic structure values $\langle c_I^2 \rangle$, averaged over the quantum motion, at appropriate reaction coordinate positions.

The variation of the TS structure with reaction asymmetry is thus described by the slope of the Brønsted coefficient, α_o', which is the derivative of eq 2.6 with respect to ΔG_{RXN} evaluated for the symmetric reaction. In this manner, α for the FER in eq 2.3 is linearly related to the reaction asymmetry

$$\alpha = \frac{1}{2} + \alpha_o' \Delta G_{RXN} \tag{2.7}$$

where $\alpha_o = {}^1/_2$ is the zero-order coefficient. The derivative of eq 2.6 yields

$$\alpha_o' = \frac{1}{2} \frac{1}{\langle c_I^2 \rangle_o^{\ddagger} - \langle c_I^2 \rangle_o^{R}} \left. \frac{\partial (\langle c_I^2 \rangle^{\ddagger} - \langle c_I^2 \rangle^{R})}{\partial \Delta G_{RXN}} \right|_o \tag{2.8}$$

Here α_o' describes the rate of change of the TS electronic structure relative to that of the reactant with respect to reaction asymmetry, evaluated for the symmetric case, $\langle c_I^2 \rangle_o^{\ddagger} - \langle c_I^2 \rangle_o^{R}$, and that rate is normalized by the TS−reactant difference in electronic structure evaluated for the symmetric case, $\langle c_I^2 \rangle_o^{\ddagger} - \langle c_I^2 \rangle_o^{R}$, in the denominator. As shown in ref 26b, and important for our subsequent analysis, the derivatives in eq 2.8 can be expressed in terms of force constants of the free energy along the reaction coordinate, k_R and $k^{\ddagger}$, at the reactant and TS positions, and the reaction coordinate distance between the reactant and product $\Delta\Delta E$ (cf. eq 1.5 of ref 26b)

$$\alpha_o' = \frac{1}{\Delta\Delta E^2} \left(\frac{1}{k^{\ddagger}} + \frac{1}{k_R} \right) \tag{2.9}$$

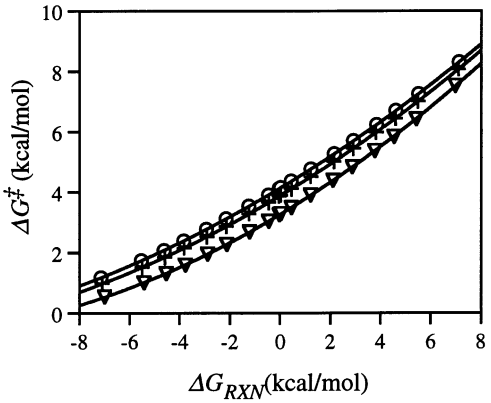

Figure 5. Free energy relationship $\Delta G^{\ddagger}$ versus ΔG_{RXN} for H (▽), D (+), and T (○). Solid lines are fits to eq 2.3 ($\Delta G_{oH}^{\ddagger} = 3.27$ kcal/mol, $\alpha_{oH}' = 0.031$ mol/kcal, $\Delta G_{oD}^{\ddagger} = 3.88$ kcal/mol, $\alpha_{oD}' = 0.025$ mol/kcal, $\Delta G_{oT}^{\ddagger} = 4.14$ kcal/mol, $\alpha_{oT}' = 0.024$ mol/kcal). The range of ΔG_{RXN} represents the relevant range for each isotope for which an activation barrier exists, e.g., for reactions in which reactant and product encounter complexes are present.

where the explicit expressions for the force constants can be decomposed into isotope-independent and -dependent contributions (cf. eq 2.1)

$$k_R = \left(\frac{\partial^2 G_{min}}{\partial \Delta E^2} + \frac{\partial^2 ZPE}{\partial \Delta E^2} \right)\Big|_R \qquad k^{\ddagger} = -\left(\frac{\partial^2 G_{min}}{\partial \Delta E^2} + \frac{\partial^2 ZPE}{\partial \Delta E^2} \right)\Big|^{\ddagger} \tag{2.10}$$

The separation $\Delta\Delta E = \Delta E_P - \Delta E_R$ and the curvatures k_R and $k^{\ddagger}$ are independent of reaction asymmetry, consistent with the analysis and formalism presented in the derivation of the adiabatic PT FER.[26a]

Both $\Delta G_o^{\ddagger}$ and α_o' are isotope-dependent. The calculated activation free energy $\Delta G^{\ddagger}$ versus reaction free energy ΔG_{RXN} profiles for H, D, and T are plotted in Figure 5 and indicate, via eq 2.3, a larger intrinsic barrier and smaller α_o' for a heavier isotope ($\Delta G_{oH}^{\ddagger} = 3.27$ kcal/mol; α_{oH}' 0.031 mol/kcal; $\Delta G_{oD}^{\ddagger} = 3.88$ kcal/mol; $\alpha_{oD}' = 0.025$ mol/kcal; $\Delta G_{oT}^{\ddagger} = 4.14$ kcal/mol; $\alpha_{oT}' = 0.024$ mol/kcal). We now turn to the explanation of these trends, beginning with the intrinsic barrier.

2b.1. Intrinsic Barrier $\Delta G_o^{\ddagger}$. In the adiabatic PT picture, the isotope dependence of the intrinsic free energy barrier $\Delta G_o^{\ddagger}$ given by eq 2.4 is apparent in Figure 4a, where the symmetric reaction difference in barrier heights is due solely to the difference in ZPE between H and D

$$\Delta G_{oD}^{\ddagger} - \Delta G_{oH}^{\ddagger} = Z_{oD}^{\ddagger} - Z_{oD}^{R} - Z_{oH}^{\ddagger} + Z_{oH}^{R} = \Delta ZPE_{oD}^{\ddagger} - \Delta ZPE_{oH}^{\ddagger} \tag{2.11}$$

Recall that the ZPE contains both that of isotope *L* and that of the H-bond vibrational mode. The latter's contribution to eq 2.4 is actually a positive contribution (+0.4 kcal/mol) to the ZPE difference $\Delta ZPE_o^{\ddagger}$ because the H-bond mode in the TS has a higher frequency than in the reactant (cf. section 2a). This difference is, however, smaller in magnitude than the negative ZPE difference associated with, for example, the proton vibrational mode (−2.5 kcal/mol). This negative value results from a larger proton vibrational frequency in the reactant compared with that at the TS, where the proton is delocalized in a double well. Thus, $\Delta ZPE_o^{\ddagger}$ is overall negative (−2.1 kcal/mol). As shown in Figure 4c, this ZPE difference decreases as

the mass of transferring particle L increases, as one would expect from a ZPE $\propto 1/\sqrt{m_L}$ mass dependence. The ZPE mass dependence will be discussed further in section 2b.3.

2b.2. α'_o. The isotope dependence of the Brønsted slope α'_o is most conveniently discussed via eq 2.9. In the denominator, the difference between H and D for the separation $\Delta\Delta E$ of the product and reaction solvent coordinate values is small (~2%, cf. Figures 4a and 4b), and so the isotopic dependence of α'_o is predominantly determined by the isotopic difference in the TS and reactant curvatures $k^{\ddagger}$ and k_R. As discussed in section 3b, the contribution from k_R is not completely negligible, but it will be shown there that the TS curvature effect is dominant in the isotope dependence of α'_o. The latter's difference in TS curvature between H and D (cf. eq 2.10)

$$k_D^{\ddagger} - k_H^{\ddagger} = \frac{\partial^2 \mathrm{ZPE}}{\partial \Delta E^2}\Big|_H^{\ddagger} - \frac{\partial^2 \mathrm{ZPE}}{\partial \Delta E^2}\Big|_D^{\ddagger} \qquad (2.12)$$

is then given by the isotopic difference in ZPE curvature at the TS, and from Figure 4a,b, $k_H^{\ddagger} < k_D^{\ddagger}$. Thus, $\alpha'_{oH} > \alpha'_{oD}$ because the TS ZPE curvature for H exceeds that for D. That this curvature is greater for H is perhaps most intuitively clear from the fact that the magnitude of the difference between the ZPE at the symmetric reaction TS and that in the reactant region will always be larger for the lighter H than for the heavier D (cf. Figure 4).

It is important to relate the above results involving the force constants to the qualitative description given at the end of section 2a for the isotope-dependent decrease of the activation barrier height with increasing reaction asymmetry: for increasing asymmetry, the TS location $\Delta E^{\ddagger}$ shifts away from $\Delta E = 0$, increasing the ZPE contribution to $\Delta G^{\ddagger}$; the latter contribution is then progressively more similar to that of the reactant (or product), and the KIE declines. We can make this connection in several steps. The first is to note that from the first member of eq 2.6, its derivative α' can be written as

$$\alpha' = \frac{\partial^2 \Delta G^{\ddagger}}{\partial^2 \Delta G_{RXN}} = \frac{1}{\Delta\Delta E}\frac{\partial(\Delta E^{\ddagger} - \Delta E_R)}{\partial \Delta G_{RXN}} \qquad (2.13)$$

where we have used $\Delta\Delta E = \Delta E_P - \Delta E_R$, which is independent of ΔG_{RXN} (cf. eq 2.9). We henceforth focus only on the TS contribution because its isotope dependence is dominant. The required slope of the TS location $\Delta E^{\ddagger}$ with ΔG_{RXN} follows from eq 5.33 in ref 26a (which also applies in the full treatment including the H-bond coordinate):

$$\Delta E^{\ddagger} = \frac{\Delta G_{RXN}}{k^{\ddagger}\Delta\Delta E} \qquad (2.14)$$

This shift of position of the TS location in the solvent coordinate $\Delta E^{\ddagger}$ changes with reaction asymmetry was already apparent in Figure4a,b,, and we now analyze it more quantitatively. Figure 6a displays the variation of the TS location in the solvent coordinate $\Delta E^{\ddagger}$ with ΔG_{RXN} for both H and D. The ~2-fold difference in slopes is clearly evident with the larger slope for H and smaller slope for D. This 2-fold difference is predominantly due to the difference in the TS curvature $k_D^{\ddagger} > k_H^{\ddagger}$, because the slope is inversely related to $k^{\ddagger}$ (cf. eq 2.14) because $\Delta\Delta E$ is only weakly isotope-dependent. For later discussion (section 4b) of the correlation of $\Delta E^{\ddagger}$ with TS structure, Figure 6b displays the TS electronic structure versus reaction asymmetry.

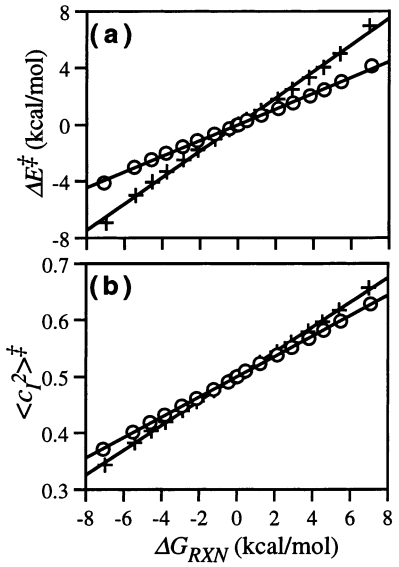

Figure 6. (a) Variation in the TS position along the reaction coordinate $\Delta E^{\ddagger}$ versus ΔG_{RXN} for H (+) and D (○). The lines are linear fits to the calculations, with the slope = 0.94 for H and = 0.56 for D. (b) Quantum average of the contribution of the product ionic VB state to the electronic structure at the TS versus reaction asymmetry, H (+) and D (○).

In the second step, we focus on the TS ZPE, which is that in Figure 4c evaluated at $\Delta E^{\ddagger}$, $\mathrm{ZPE}^{\ddagger} = \mathrm{ZPE}(\Delta E^{\ddagger})$, and whose variation with reaction asymmetry directly correlates with the variation of $\Delta E^{\ddagger}$ via eq 2.14 (cf. eq 5.24 in ref 26a),

$$\mathrm{ZPE}^{\ddagger} = \mathrm{ZPE}(\Delta E^{\ddagger}) = Z_{m,o}^{\ddagger} \mp a^{\ddagger}\Delta E^{\ddagger} - \frac{b^{\ddagger}}{2}\Delta E^{\ddagger 2} \qquad (2.15)$$

where $a^{\ddagger}$ and $b^{\ddagger}$ are the first and second derivatives, respectively, of ZPE with respect to ΔE, evaluated at the reaction coordinate TS position for the symmetric reaction. (The $\mp$ in eq 2.15 ensures that the ZPE is minimal for $\Delta E = 0$ and increases as $|\Delta E|$ increases.) The second-order dependence on reaction asymmetry, given by the last term in eq 2.15, though negative and, thus, decreasing with increasing reaction asymmetry, is not as significant as the linear term (cf. Figure 4). The reaction asymmetry dependence in eq 2.14 together with eq 2.15 clearly shows that $\mathrm{ZPE}^{\ddagger}$ increases with reaction asymmetry.

From eq 2.15, the initial rate of increase in $\mathrm{ZPE}^{\ddagger}$ with reaction asymmetry is the derivative with respect to ΔG_{RXN} evaluated for the symmetric reaction

$$\frac{\partial \mathrm{ZPE}^{\ddagger}}{\partial \Delta G_{RXN}}\Big|_o = \frac{a^{\ddagger}}{k^{\ddagger}\Delta\Delta E} \qquad (2.16)$$

The denominator in eq 2.16 is the same as in eq 2.14, such that eq 2.16 can be substituted into eq 2.13, plus its analogous expression for the reactant region (see Appendix A, eq A.5)

$$\alpha'_o = \frac{1}{\Delta\Delta E}\frac{\partial(\Delta E^{\ddagger} - \Delta E_R)}{\partial \Delta G_{RXN}} = \frac{1}{\Delta\Delta E}\left[\frac{1}{a^{\ddagger}}\frac{\partial \mathrm{ZPE}^{\ddagger}}{\partial \Delta G_{RXN}}\Big|_o - \frac{1}{a}\frac{\partial \mathrm{ZPE}^{R}}{\partial \Delta G_{RXN}}\right] \qquad (2.17)$$

where a is the first derivative of the ZPE in the reactant region.

The isotope-dependent difference of α'_o (see Appendix A, eq A.6)

$$\alpha'_{oH} - \alpha'_{oD} = \frac{1}{\Delta\Delta E}\left[\frac{1}{a^{\ddagger}}\left(\left.\frac{\partial ZPE^{\ddagger}}{\partial \Delta G_{RXN}}\right|_{o,H} - \left.\frac{\partial ZPE^{\ddagger}}{\partial \Delta G_{RXN}}\right|_{o,D}\right) - \left(\frac{1}{a^{H}}\frac{\partial ZPE_{H}^{R}}{\partial \Delta G_{RXN}} - \frac{1}{a^{D}}\frac{\partial ZPE_{D}^{R}}{\partial \Delta G_{RXN}}\right)\right] \quad (2.18)$$

is now explicitly described by the isotope-dependent ZPE variation at the reactant and TS with reaction asymmetry. As will be shown in section 3b, the first term in eq 2.18 is the most significant, and thus, the isotope difference $\alpha'_{oH} - \alpha'_{oD}$ is proportional to the difference in rate of increase of $ZPE^{\ddagger}$ with increasing reaction asymmetry between H and D, which is directly related to the TS curvature via eq 2.16. (Note that $a^{\ddagger}$ is isotope-independent, a property of the discontinuity at $\Delta E = 0$.[26a])

It is significant to note that the adiabatic $ZPE^{\ddagger}$ versus ΔG_{RXN} behavior just described parallels the standard view in a general way: the proton $ZPE^{\ddagger}$ is minimal for a symmetric reaction and increases with reaction asymmetry, resulting in a KIE which is maximal for $\Delta G_{RXN} = 0$ and falls off for both exo- and endothermic reactions. Again we stress that the cause of the increase in $ZPE^{\ddagger}$ for the present and standard views is quite different because the reaction coordinates and physical picture for PT are completely different. We also note that the positions of the reactant and product states, as seen in Figure 4 and explicitly present in eq 2.17, also shift upon addition of the ZPE, but this is not a major effect: the change for the reactant ZPE going from a symmetric to an asymmetric reaction is smaller than the corresponding $ZPE^{\ddagger}$ change, because the ZPE variation is largest near $\Delta E = 0$. The important net result is that the difference $ZPE^{R} - ZPE^{\ddagger}$ decreases as the reaction becomes more asymmetric.

2b.3. Further Analysis of the Intrinsic Barrier. Mass Scaling. Further analysis of the intrinsic barrier $\Delta G_o^{\ddagger}$'s isotope dependence will prove useful for our subsequent discussion of both the KIE magnitude and the Swain−Schaad relationship. The intrinsic barrier's isotope dependence given by eq 2.4 is only dependent on the difference in ZPEs (cf. eq 2.11),

$$\Delta G^{\ddagger}_{oL_2} - \Delta G^{\ddagger}_{oL_1} = \Delta ZPE^{\ddagger}_{oL_2} - \Delta ZPE^{\ddagger}_{oL_1} \quad (2.19)$$

This illustrates a key common point of connection between the present and standard perspectives: in both cases, the difference in intrinsic barrier heights is related to the difference in a ZPE between the reactant and TS between both isotopes. However, the *identity* of the ZPE contribution to the TS *differs* in the two perspectives. For example, the ZPE at the TS has no contribution from the proton for a symmetric reaction in the standard picture, whereas it does in the present picture.

We now address the mass scaling of the ZPE, which is key to many aspects of KIEs. In standard treatments, this scaling is $ZPE \propto 1/\sqrt{m}$ for the L contribution, which assumes harmonic potentials. The proton potentials in Figure 1 are not harmonic, especially *at* the TS, where there is a double well, and thus one does not expect the simple ZPE mass scaling to hold. We now explore whether there are any important consequences of this. For this purpose, the contribution in the adiabatic picture of L to the ZPE, excluding the H-bond vibration ZPE, in either the reactant or TS is calculated by subtracting off the ZPE due to the H-bond mode, the latter being taken from the relevant H-bond potentials (see Figure 3).

We focus first on the reactant region. The contribution from H to the reactant ZPE (Z^{R}_{oH}) is 3.61 kcal/mol, and assuming that $ZPE_D = ZPE_H/\sqrt{2}$, one predicts 2.55 kcal/mol for the contribution from D to Z^{R}_{oD}. This value is extremely close to the actual value of 2.62 kcal/mol. This should not be too surprising, because anharmonic potentials, e.g., Morse potentials, have a significant harmonic component for the ZPE.

Turning to the TS, the H contribution to $Z^{\ddagger}_{oH}$ is 1.15 kcal/mol and that from D to $Z^{\ddagger}_{oD}$ is 0.73 kcal/mol. If one assumes that $ZPE_D = ZPE_H/\sqrt{2}$, the latter is predicted to be 0.81 kcal/mol, a larger relative difference, ~10%, from the actual value than for the reactant region. This larger difference is to be expected, because the TS proton potential is a *very* anharmonic double well. Because, however, the D ZPE is quite small, the error is small in magnitude, 0.1 kcal/mol, an error of less than 10% in the difference $\Delta ZPE^{\ddagger}_o$ in ZPEs. We now quantify the effect this small difference has on a mass scaling of ZPEs picture for the KIE.

If we assume that all ZPEs scale according to $ZPE_L \propto 1/\sqrt{m_L}$, eq 2.19 is

$$\Delta G^{\ddagger}_{oL_2} - \Delta G^{\ddagger}_{oL_1} = \Delta ZPE^{\ddagger}_{oL_2}\left(1 - \sqrt{(m_{L_2}/m_{L_1})}\right) = \Delta ZPE^{\ddagger}_{oH}\left(\sqrt{(m_H/m_{L_2})} - \sqrt{(m_H/m_{L_1})}\right) \quad (2.20)$$

where we have scaled all differences in $\Delta G^{\ddagger}_o$ to the ZPE difference $\Delta ZPE^{\ddagger}_o$ for H in the last line. We can test this simple mass scaling by using the numerical values for the intrinsic barriers from Figure 5 for all three differences in intrinsic barrier for the H, D, and T trio and inserting them into the left-hand side of eq 2.20. One can then estimate, using eq 2.20, the difference in ZPE between reactant and TS for H $\Delta ZPE^{\ddagger}_{oH}$, whose exact numerical value is $\Delta ZPE^{\ddagger}_o = -2.10$ kcal/mol. The results are $\Delta G^{\ddagger}_{oH} - \Delta G^{\ddagger}_{oD}$ gives $\Delta ZPE^{\ddagger}_{oH} = -2.08$ kcal/mol, $\Delta G^{\ddagger}_{oH} - \Delta G^{\ddagger}_{oT}$ gives $\Delta ZPE^{\ddagger}_{oH} = -2.06$ kcal/mol, and $\Delta G^{\ddagger}_{oD} - \Delta G^{\ddagger}_{oT}$ gives $\Delta ZPE^{\ddagger}_{oH} = -2.00$ kcal/mol. The close agreement of these with the exact value as well as the minimal variation between the three values highlights an important point: the adiabatic PT picture *also* generates, from a numerical viewpoint, the mass scaling of standard KIE theory. This will prove to be especially important for the Swain−Schaad relation, which is entirely dependent on this mass scaling,[7,10,13] discussed in section 3c.

3. Kinetic Isotope Effects

We now document the claim of the Introduction that the experimentally observed KIEs thought to support the standard view also follow from the adiabatic PT perspective. We begin by recounting general adiabatic PT relations. The KIE is the ratio of individual rate constants, where each rate constant is of the form in eq 2.2. For H versus D transfer, for example, the KIE expression is

$$\frac{k_H}{k_D} = \frac{\omega_S^H}{\omega_S^D}\exp(-(\Delta G_H^{\ddagger} - \Delta G_D^{\ddagger})/RT) \quad (3.1)$$

Here $\omega_S^{H,D}$ are the reactant reaction coordinate frequencies, and $\Delta G^{\ddagger}_{H,D}$ are the free energy barriers for H and D transfer, respectively. ω_S^H and ω_S^D are nearly identical (differing only by ~2%) because the reactant region force constant is dominated by the force constant of G_{min} (cf. Figure 4), which is independent of isotope because it refers to a classical fixed protonic species;

we ignore this minor effect hereafter, and simply write

$$\frac{k_H}{k_D} \approx \exp(-(\Delta G_H^{\ddagger} - \Delta G_D^{\ddagger})/RT) \qquad (3.2)$$

Several further forms for the KIE k_H/k_D will prove useful in the subsequent discussion. The first follows from the FER analysis in section 2 and is useful for the analysis of the KIE versus reaction asymmetry behavior; with eq 2.3 for the reaction barrier, the explicit form for the KIE dependence on ΔG_{RXN} is

$$\frac{k_H}{k_D} = \exp(-(\Delta G_{oH}^{\ddagger} - \Delta G_{oD}^{\ddagger})/RT)\exp(-(\alpha'_{oH} - \alpha'_{oD})\Delta G_{RXN}^{\ 2}/2RT) \qquad (3.3)$$

whereas the second, equivalent form reexpresses the first part of this in terms of the KIE for the symmetric reaction:

$$\frac{k_H}{k_D} = \frac{k_{Ho}}{k_{Do}}\exp(-(\alpha'_{oH} - \alpha'_{oD})\Delta G_{RXN}^{\ 2}/2RT) \qquad (3.4)$$

The content of these equations is that the KIE is maximal for the symmetric reaction $\Delta G_{RXN} = 0$, given by the first term in either eq 3.3 or eq 3.4. This general feature follows because the Brønsted coefficient for a symmetric reaction is independent of isotope, $\alpha_o = {}^1/_2$ (which reflects the symmetric nature of the electronic structure of the reacting pair at the TS (cf. eq 2.5)[45]). The decrease from the maximum, characterized by a Gaussian falloff with increasing reaction asymmetry, is due to the isotope dependence $\alpha'_{oH} > \alpha'_{oD}$, discussed in section 2b.2.

In the following subsections, we determine, via evaluation of eqs 3.1−3.4, the various KIE aspects that result from the adiabatic PT picture and show that these are essentially the same as those generally thought to support the standard picture. For each particular KIE feature, we discuss its source within the adiabatic PT picture and for the most part delay a detailed comparison with the standard and other approaches until section 4.

3a. KIE Arrhenius Behavior. The Arrhenius form for the adiabatic PT KIE in eqs 3.1−3.4 is consistent with the first set of experimental results (i) stated in the Introduction, and the general form for the KIE is identical to that of the standard picture (i.e., the adiabatic PT eq 3.2 is similar to the standard eq 1.2), despite significant differences in ingredients between the present and standard picture. The adiabatic PT rate constant eq 3.2 has its temperature dependence governed by a temperature-independent $\Delta G^{\ddagger}$. Although it is true that additional temperature dependence is in principle present in both the prefactor and $\Delta G^{\ddagger}$ of the above KIE expressions, they are negligible for highly polar solvents.[8,47,48]

3b. KIE Magnitude and Variation with Reaction Asymmetry. The KIE behavior versus reaction asymmetry in the adiabatic PT perspective follows directly from insertion of the isotopic difference between the FER curves from Figure 5 into eq 3.2. Figure 7 displays the resulting H versus D KIE (T = 300 K). The calculated KIE is maximum at $\Delta G_{RXN} = 0$ and drops off symmetrically as the reaction asymmetry is increased. The maximum KIE for the symmetric reaction and the KIE magnitude throughout the whole range for adiabatic PT are both consistent with experimental observations, (ii) and (iii), respectively, of the Introduction. We briefly recount here the origin of the aspects in the adiabatic PT picture.

In the adiabatic PT view, the magnitude of the intrinsic KIE is directly related to the isotopic difference TS−R ZPE

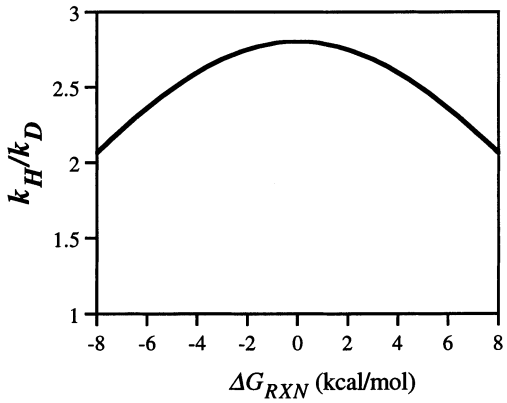

Figure 7. KIE k_H/k_D versus ΔG_{RXN} using FERs in Figure 5 (T = 300 K).

difference $\Delta ZPE_o^{\ddagger} = Z_o^{\ddagger} - Z_o^R$ (see eqs 2.11 and 2.19), whose unusual feature is the presence of the ZPE for the bound proton vibration at the solvent coordinate TS. The mass dependence of $\Delta ZPE_o^{\ddagger}$ can be understood most simply from the mass-scaling of ZPEs discussed in section 2b.3. (We will return to the issue of the KIE magnitude in section 4a.)

We now turn to the Gaussian falloff from maximum of the KIE dependence on ΔG_{RXN}, which is due to the isotope dependence of the Brønsted coefficient derivatives $\alpha'_{oH} > \alpha'_{oD}$, as noted in the introduction of this section below eq 3.4. From eqs 2.9 and 2.10, this isotope dependence requires attention to the force constants at the reactant and TS solvent coordinate positions in the adiabatic PT picture.

As discussed in section 2b.2, the isotope difference $\alpha'_{oH} - \alpha'_{oD}$ has its qualitative origin, the essential point, in the greater magnitude of the force constant $k^{\ddagger}$ in the solvent coordinate for D than for H, which in turn reflects the stronger curvature of the H ZPE at the TS compared to that for D (cf. eq 2.12). A quantitative analysis is, however, complicated by further smaller effects related to the isotope dependence of the reactant force constant k_R and the distance $\Delta\Delta E$ between the product and reactant solvent coordinate values. We now address this.

From eq 2.9, we can write

$$\alpha'_{oH} - \alpha'_{oD} = \frac{1}{k_R^H \Delta\Delta E_H^{\ 2}}\left(1 - \chi + \frac{k_R^H}{k_H^{\ddagger}} - \chi\frac{k_R^D}{k_D^{\ddagger}}\right) \qquad (3.5)$$

where the factor

$$\chi = \frac{k_R^H \Delta\Delta E_H^{\ 2}}{k_R^D \Delta\Delta E_D^{\ 2}} \qquad (3.6)$$

is numerically close to one, $\chi = 0.94$. The difference from unity, however, is significant: setting $\chi = 1$, gives $\alpha'_{oH} - \alpha'_{oD} = 0.0028$ mol/kcal, which is far from the actual value $\alpha'_{oH} - \alpha'_{oD} = 0.0046$mol/kcal. The first two terms in eq 3.5 correspond to the isotopic difference in reactant curvatures, which contributes (=0.0013) 28% to the total difference, whereas the last two terms correspond to the isotopic difference in the TS curvatures, which contribute (=0.0033) 72%. In summary, the isotope difference $\alpha'_{oH} - \alpha'_{oD}$ is *primarily* determined via eq 3.5 by the isotopic difference in ZPE curvatures in the TS and reactant regions (cf. eq 2.18), with the dominant contribution from the former.

3c. Swain−Schaad Relationship. We now turn to the Swain−Schaad relationship, which has been an important

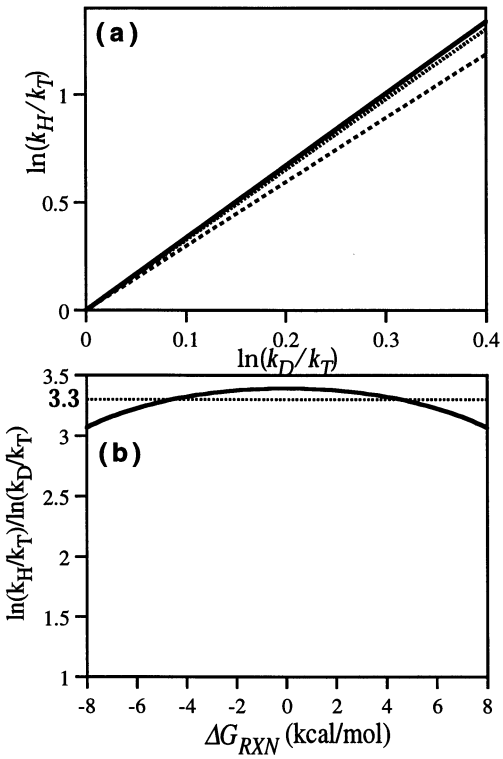

Figure 8. (a) $\ln(k_H/k_T)$ versus $\ln(k_D/k_T)$ for varying T with for three values of reaction asymmetry constant: $\Delta G_{RXN} = 0$ (solid line), $|\Delta G_{RXN}| = 3.5$ kcal/mol (dotted line), and $|\Delta G_{RXN}| = 7$ kcal/mol (dashed line). The slopes of the lines are 3.41, 3.39, and 3.16, respectively. (b) Swain−Schaad slope $\ln(k_H/k_T)/\ln(k_D/k_T)$ versus reaction asymmetry calculated using the free energy relationships in Figure 5 ($T = 300$ K).

experimental probe for PT reaction KIEs.[4,10,13] Here we examine one of its forms

$$\ln(k_H/k_T) = 3.3 \ln(k_D/k_T) \tag{3.7}$$

This relationship assumes the mass correlation of ZPE discussed in section 2b.3 ZPE $\propto 1/\sqrt{m}$ to relate the H, D, and T ZPEs in eq 1.2. (Significant deviations from the predicted relationship for primary (and secondary) KIEs have been used as a signature of proton tunneling (nonadiabatic PT).[4,10,13,49]) We now examine the adiabatic PT predictions.

Figure 8a displays the calculated adiabatic PT $\ln(k_H/k_T)$ versus $\ln(k_D/k_T)$, determined by varying the temperature for three reaction asymmetries. The behavior for each reaction asymmetry is linear with a slope close to that of the expected value ~3.3. The slope is plotted versus reaction asymmetry in Figure 8b and shows little variation from eq 3.7. Thus, conventional Swain−Schaad behavior also follows from the adiabatic PT picture. We now analyze the reasons for this.

From the ΔG_{RXN}-dependent form in eq 3.3 for the KIE, the natural logarithm of the H/D KIE is

$$\ln\left(\frac{k_H}{k_D}\right) = (\Delta ZPE^{\ddagger}_{oD} - \Delta ZPE^{\ddagger}_{oH} - \Delta G_{RXN}{}^2(\alpha'_{oH} - \alpha'_{oD})/2)/RT \tag{3.8}$$

where eq 2.11 was used for the intrinsic barrier difference. The ratio of natural logarithms for the Swain−Schaad relation in eq 3.7 is then

$$\ln\left(\frac{k_H}{k_T}\right)/\ln\left(\frac{k_D}{k_T}\right) = \frac{\Delta ZPE^{\ddagger}_{oT} - \Delta ZPE^{\ddagger}_{oH} - \Delta G_{RXN}{}^2(\alpha'_{oH} - \alpha'_{oT})/2}{\Delta ZPE^{\ddagger}_{oT} - \Delta ZPE^{\ddagger}_{oD} - \Delta G_{RXN}{}^2(\alpha'_{oD} - \alpha'_{oT})/2} \tag{3.9}$$

A first significant point is that the adiabatic PT form in eq 3.9 has the same important feature as the standard picture, via eq 1.2: the Swain−Schaad relation is independent of temperature.

To examine more closely the second important point, the magnitude of the Swain−Schaad slope, we examine first the symmetric case $\Delta G_{RXN} = 0$, for which the adiabatic PT eq 3.9 shows that the magnitude is related solely to the difference in reactant and TS ZPEs. In section 2b.3, these differences in ZPEs were shown to obey the same mass scaling used to derive the Swain−Schaad relations (cf. eq 2.20), and hence the maximum of the plot in Figure 8 is close to the traditionally expected value.

Figure 8 shows that there is a variation, in the adiabatic PT perspective, of the Swain−Schaad slope with reaction asymmetry. This can be understood by examining asymmetric reactions, for which the reactant, product, and TS positions differ between H, D, and T, because the variation of ZPE for each isotope along the reaction coordinate ΔE is different (see Figure 4c). Consequently, the critical point ZPEs are not those of the same proton potentials for a given ΔG_{RXN}. Therefore, the ratio $\ln(k_H/k_T)/\ln(k_D/k_T)$ should not be constant throughout the entire range of ΔG_{RXN}. But the net effect of these shifts is minimal, as displayed in Figure 8.

Thus, close adherence to the Swain−Schaad relationship is expected in the adiabatic PT picture, largely due to the mass scaling described above. Large departures from the Swain−Schaad relationship for *tunneling* PT[4] are discussed elsewhere.[14]

4. Further Discussion of the Interpretation of Kinetic Isotope Effects

We have already repeatedly emphasized in previous sections several important fundamental distinctions between the adiabatic PT and the standard view. Despite these distinct differences in physical perspective between adiabatic PT and the standard W−M picture, it is important to now emphasize that a remarkable *general* similarity exists between the two perspectives. For adiabatic PT, the KIE for the symmetric reaction is dependent on the difference in magnitude of the TS-reactant difference $\Delta ZPE^{\ddagger}_{o}$, and the variation in KIE with reaction asymmetry is due to the variation of TS ZPE (and structure). These two points, in fact, are shared with the W−M picture. Recall that in the latter, the $ZPE^{\ddagger}$ variation also determines the KIE (cf. eq 1.2), although its source is different from that of the adiabatic PT picture. In what follows, the numerical and physical differences between the two perspectives are further enumerated. In particular, the interpretation of the KIE versus reaction asymmetry behavior is discussed. We begin with a reinterpretation of the magnitude of the KIE and how it compares with the standard picture.

4a. Magnitude of the Primary Kinetic Isotope Effect. The adiabatic PT maximum KIE in Figure 7 is in the range of KIEs commonly expected in the standard W−M picture, item (iii) in the Introduction. It is somewhat smaller than the higher KIEs 6−10 that one would expect with the standard view. We now address the maximal adiabatic PT H/D KIE magnitude that can result and how it compares with the standard picture.

From eqs 3.3 and 3.4, the maximum H/D KIE is that of the symmetric reaction

$$\frac{k_{\mathrm{Ho}}}{k_{\mathrm{Do}}} = \exp[-(\Delta G^{\ddagger}_{\mathrm{oH}} - \Delta G^{\ddagger}_{\mathrm{oD}})/RT] \qquad (4.1)$$

From eq 2.20, where the ZPEs between H and D are mass-scaled, this maximal KIE can be written in terms of the proton ZPE:

$$\frac{k_{\mathrm{Ho}}}{k_{\mathrm{Do}}} = \exp\left[-\Delta \mathrm{ZPE}^{\ddagger}_{\mathrm{oH}}\left(1 - \sqrt{\frac{1}{2}}\right)/RT\right] \qquad (4.2)$$

(Equation 4.2 is also used[1,5,7] as an estimate for the KIE in the standard W−M picture (cf. eq 1.2).) The different symmetric reaction KIE limits for the adiabatic PT and W−M pictures is entirely due to their different views of the TS reaction and transverse coordinates: for a symmetric reaction, there is always a finite proton TS ZPE contribution for adiabatic PT, whereas the proton TS ZPE is zero ($Z^{\ddagger}_{\mathrm{oH}} = 0$) in the W−M description. The maximum KIE is thus always smaller in the adiabatic PT view.

Further analysis requires attention to the magnitude of H stretch frequencies. In an H-bond with sufficient strength, the A−H stretch frequency has a significant red shift, e.g., a frequency ω_{OH} of ∼3200 cm^{-1} for an O···O H-bond distance of ∼2.7 Å.[25] (This is a modest H-bond; stronger H-bonds will have ω_{OH} < 3200 cm^{-1} compared to a "free" OH stretch frequency ∼3600 cm^{-1}.[25] PT in a weaker O···O H-bond with a larger equilibrium separation will most likely involve tunneling.[26,38]) With a reactant frequency ω_{OH} = 3200 cm^{-1}, the W−M picture gives $k_{\mathrm{H}}/k_{\mathrm{D}} \approx 10$ at 300 K. Turning to other acids, a similar red shift is observed for N−H vibrations in H-bonds with ω_{NH} ∼ 3000 cm^{-1}.[25] Carbon acids will, of course, have smaller red shifts, but the C−H stretch frequency itself (∼3000 cm^{-1}) is typically less than that for O−H. Hence, for all common acids $k_{\mathrm{H}}/k_{\mathrm{D}} \approx 10$ is a good estimate for the maximum KIE for the standard picture, excluding tunneling.

Turning to adiabatic PT (with an appropriately small proton barrier height such that neither the proton nor deuteron tunnel), the TS ZPE for the proton is ∼1 kcal/mol for H and ∼0.7 kcal/mol for D. Using ω_{R} ∼3200 cm^{-1} as the maximum reactant frequency and ∼1 kcal/mol ZPE for H at the TS, the maximum KIE without tunneling is ∼6 at 300 K, a value obviously lower than that for the W−M picture. An experimental prescription to distinguish these perspectives would be to find the maximum observed KIE for which the reaction is known not to involve tunneling. Unfortunately, although the possible distinction between tunneling and nontunneling PT reactions has generated intensive experimental effort;[1,4,5,7,12,13] this is not at all straightforward: the difficulty is that the magnitude of tunneling KIEs overlaps with that of nontunneling, especially in the 5−10 range.[50] For a more promising arena to experimentally probe the difference between perspectives, we now look to the other limit of the KIE, where tunneling is less likely to be present.

To begin, the first key remark to make is that the complete loss of the ZPE in the reactant going to the TS in a symmetric reaction in the standard picture also limits the *minimum* symmetric reaction KIE value. From eq 4.2, the minimum value results from the smallest reactant proton stretch frequency ω_{R} one could have and still have PT. A reactant proton stretch frequency of 2300 cm^{-1} gives $k_{\mathrm{H}}/k_{\mathrm{D}} \approx 5$ for the standard picture. Such a value, however, would obviously correspond to a *very* strong H-bond,[25] and it is questionable that smaller reactant proton frequencies would be plausible while still permitting activated PT: the reaction barrier for interconversion of proton states in the standard picture would be expected to be quite small.[51] Consequently, the expected $k_{\mathrm{H}}/k_{\mathrm{D}}$ range for a symmetric reaction in the standard picture is ∼5−10. In the adiabatic PT approach, however, a finite symmetric reaction TS ZPE reduces the minimum value to less than 3 (cf. Figure 7).

The disparity between the two perspectives should thus be experimentally observable, especially for the lower KIE. In this connection, we note that a $k_{\mathrm{H}}/k_{\mathrm{D}}$ versus reaction asymmetry plot has been determined for a variety of PT systems, and the $k_{\mathrm{H}}/k_{\mathrm{D}}$ maximum ranges from 3 to 10,[2,5,52] the lower limit being the key focus here. Included in the lower part of this KIE range is an enzymatic PT,[2c] a nonenzymatic PT,[2e] and an excited-state PT from a photoacid to a water molecule.[52] All three have a $k_{\mathrm{H}}/k_{\mathrm{D}}$ maximum ∼3−4, a value not obtainable with the standard picture, at least within a linear H-bond model.[53]

We need to stress that the above discussion has ignored vibrational contributions other than the AH stretch. We have already discussed in section 2 the H-bond stretch contribution to $\Delta \mathrm{ZPE}^{\ddagger}$, where it was shown that a H-bond frequency is larger for the TS compared than for the reactant. However, because this H-bond frequency difference does not significantly change between H and D transfer, the KIE magnitude is unaffected. A vibration that *is* isotope-dependent is the AH bending vibration. Loss of bending vibrations going from reactant to TS has been postulated to account for the possibility of increased KIEs without tunneling.[1,5,7] However, when PT occurs within an H-bonded complex, the *loss* of a bending vibration at the TS does not seem likely.[7] Instead, the H bending vibrational frequencies increase with increasing H-bond strength,[25] and thus are expected (if any change is expected) to increase going from the reactant to the TS due to a shorter and tighter H-bond vibration in the TS compared with the reactant. Consequently, a bending mode would decrease the reactant/TS ZPE difference between H and D and would thus decrease the KIE magnitude.[54]

The discussion just presented has been for adiabatic PT in a linear H-bonded complex (as specified in section 2a), with a reasonably strong H-bond, as noted in section 1. It is important, however, to briefly pause to put this into further perspective. Figure 9a displays a model calculation for the adiabatic free energies for PT in a linear H-bonded complex that includes in-plane bending motion. Here a definite interaction between the H bend and stretch in the first two vibrationally excited states is seen, but without any impact on the system ground vibrational state ($\upsilon_{\mathrm{H}} = 0$), just as assumed in our treatment. The key feature is that the bend frequency does not change significantly on going from reactant to TS, whereas the splitting between the ground state and single excitation in the stretch significantly decreases going from reactant to TS. The ground state adiabatic character is further confirmed by examination of the proton wave function (not shown), which is strongly delocalized, as in Figure 1a. The situation is, however, changed for a slightly larger H-bond separation, but for a complex that is significantly bent, in Figure 9b.[55] Here the PT has significant nonadiabatic character, as indicated by the avoided crossing of the ground level and first vibrationally excited level involving the stretch (the diabatic crossing curves at the TS are those of the proton stretches in the reactant and the product). In addition, excited stretch and bend coupling is visible to the left and right of the TS. The nonadiabatic character is confirmed by examination of the ground state proton wave function (not shown), which is largely localized in both the reactant and product wells. Thus, the adiabatic description for the ground-state reaction does not

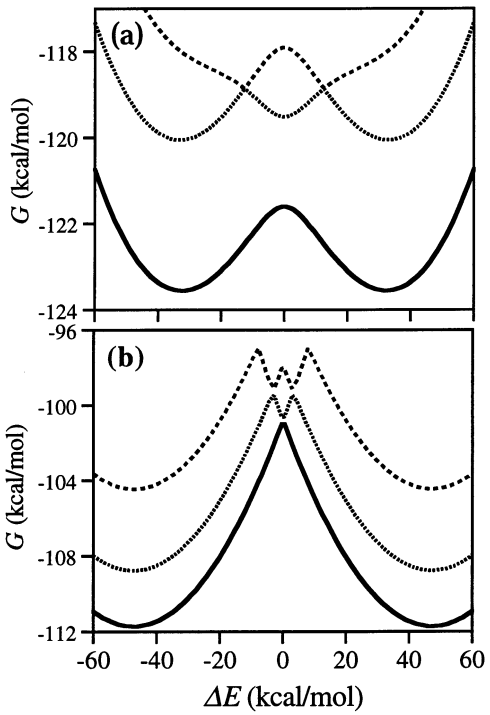

Figure 9. Proton adiabatic free energy curves for a symmetric PT reaction for the ground (solid line), first (dotted line), and second (dashed line) excited proton vibrational states (including stretch and harmonic bend) for a fixed A−B H-bond distance Q. In the reactant and product regions, the first excited state is a bending excitation, whereas the second excited state is a stretching excitation. At the TS, the situation is reversed: the first excited state is a stretching excitation, whereas the second excited state is a bending excitation. (a) A linear H-bond H−A−B angle = 0° and short H-bond distance Q = 2.55 Å, with $\omega_{stretch}$ = 2600 cm^{-1} and ω_{bend} = 1200 cm^{-1}. (b) A slightly larger A−B separation Q = 2.6 Å, but with a strongly bent H-bond H−A−B angle = 30°, with $\omega_{stretch}$ = 2900 cm^{-1} and ω_{bend} = 1200 cm^{-1}. For these calculations, the H-bond model of ref 26 is used, except that the A−B H-bond separation is held fixed while a harmonic in-plane bending motion is included. In the bent system, the stretch direction (A−H or H−B) of the two VB potentials is out of line with the A−B direction, i.e., the angle H−A−B in the reactant and H−B−A in the product is nonzero. The stated H stretch and bend frequencies are those in the reactant and product VB states.

apply, and, as for the first case, coupling with the bend must be taken into account in excited-state reactions. The violation of the adiabaticity condition for the ground-state reaction has its origin in the feature that even though the A−B separation in the second case is only slightly larger than for the first case, the bent configurations of reactant and product result in a larger separation over which the proton must be transferred.[56] This kind of consequence was already pointed out in refs 19b and 19c, where it was noted that nonadiabatic tunneling PT (rather than adiabatic PT) is to be expected in, e.g., intramolecular proton transfer with bent complexes, involving longer effective proton-transfer distances imposed by the molecular geometry.

4b. KIE and Transition State Structure. One of the most important applications from a chemical point of view of the standard picture is the use of measured KIE values to infer the structure of the reaction TS. The maximum KIE in Figure 7 is associated with a symmetric TS, and the KIE magnitude falloff with increasing reaction asymmetry correlates to asymmetric transition states. Thus, a small observed KIE for an exothermic reaction could be interpreted as partial H motion in the TS for the H reaction. More quantitatively, the TS structure is characterized by the Brønsted coefficient α[2,5,7,28] (see discussion in section 2b).

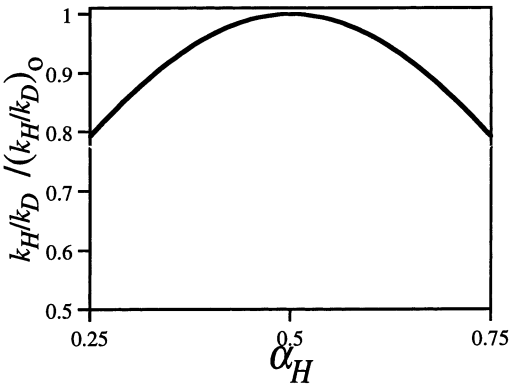

Figure 10. Relative KIE $k_H/k_D/(k_H/k_D)_o$ versus proton Brønsted coefficient α_H for the KIE behavior in Figure 7.

Because the adiabatic PT picture has the solvent coordinate as the reaction coordinate, and both the proton and H-bond coordinates are quantum rather than classical, it is not perhaps immediately obvious how such notions would survive. As we now show, these concepts, suitably generated, are a natural consequence of the adiabatic PT picture. To begin exploration of the KIE-TS structure behavior for adiabatic PT, we first consider the relative rate of KIE falloff with reaction asymmetry compared to the symmetric case, eq 3.4, which we rewrite using the fact that α, and hence the TS structure, is linearly related to the reaction asymmetry via eq 2.7 where α'_o describes the rate of TS structure change with reaction asymmetry. By substitution for ΔG_{RXN} in eq 3.4, this gives a Gaussian KIE−TS structure behavior

$$\left(\frac{k_H}{k_D}\right)\Big/\left(\frac{k_H}{k_D}\right)_o = \exp\left[-\frac{\gamma\left(\alpha_H - \frac{1}{2}\right)^2}{2\quad RT}\right] \qquad (4.3)$$

where γ is defined as

$$\gamma = \frac{(\alpha'_{oH} - \alpha'_{oD})}{\alpha'^{\,2}_{oH}} \qquad (4.4)$$

and α_H is the reference TS structure. (Note that eq 4.3 is a general expression for *any* FER of the form in eq 2.3.) γ is the scale factor that describes the sensitivity of KIE variation with α_H. Figure 10 displays the behavior in eq 4.3 for the adiabatic PT systems in Figures 5 and 7.

In adiabatic PT, the Brønsted coefficient for PT α_H is described via eq 2.6 in terms of the contribution of the reactant and product VB states to the quantum-averaged TS electronic structure (e.g., $\langle c_l^2 \rangle$). To expand on the α−TS structure correlation, we now consider a more geometric picture. Before effecting this, we review the traditional approach.

4b.1. Traditional Approach. Traditionally, model potential reaction surfaces for gas-phase H atom transfers have been analyzed by finding the maximum along the minimum energy path (MEP), the TS; then the frequencies parallel and perpendicular to the reaction path were obtained to evaluate the KIE.[57] A bond energy−bond order (BEBO) perspective was often used, where the MEP is described by the bond order n of the bond being formed, and hence, the nuclear geometry and frequencies (e.g., that of Q and q) along that classical reaction path are a function of n. KIE analysis proceeds by finding the maximum point along that reaction path, i.e., the bond order $n^{\ddagger}$ of the TS, and its corresponding parallel and perpendicular frequencies.[57] The connection between α and the TS structure in the standard

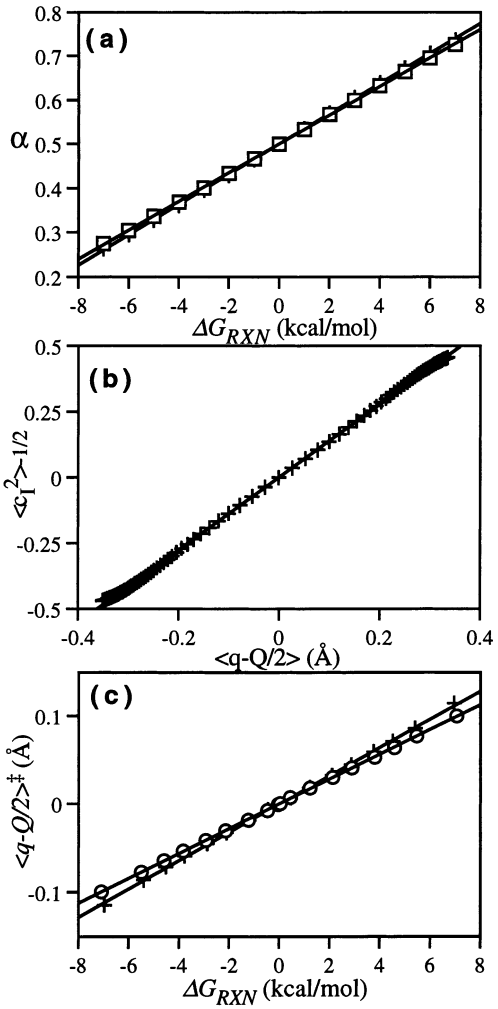

Figure 11. (a) Brønsted coefficient α versus reaction asymmetry ΔG_{RXN} using the quantum-averaged VB ionic electronic structure component $\langle c_I^2\rangle$ in eq 2.6 (□) and the quantum-averaged distance of the proton to the H-bond center $\langle q - Q/2\rangle$ in eq 4.5 (+). (b) $\langle c_I^2\rangle - {}^1/_2$ versus $\langle q - Q/2\rangle$. (c) Quantum average $\langle q - Q/2\rangle^{\ddagger}$ of the TS proton distance to the H-bond center versus ΔG_{RXN}, H (+) and D (○). Lines are linear fits to the points.

picture thus has as its origin the relationship $\alpha = n^{\ddagger}$;[44] because $n^{\ddagger}$ determines the TS geometry and frequencies, α is also directly linked with TS structure.

4b.2. Adiabatic PT Approach. For adiabatic PT, we have previously shown[26b] that progression along the solvent reaction coordinate, which is correlated with a change of electronic structure $\langle c_I^2\rangle$, also corresponds to a quantum average reaction path similar to that predicted by the BEBO PT picture for H atom transfer in the gas phase. We now demonstrate that a similar connection of α with explicit TS structure geometry is also achieved with adiabatic PT.

The relation of α to the quantum average over the proton and H-bond vibrations of the A−H and A−B separations at the TS, reactant, and product positions is derived in Appendix B (see eq B.5) to be

$$\alpha = \frac{\langle q - Q/2\rangle^{\ddagger} - \langle q - Q/2\rangle^{R}}{\langle q - Q/2\rangle^{P} - \langle q - Q/2\rangle^{R}} \tag{4.5}$$

where the structural element $\langle q - Q/2\rangle$ is the quantum-averaged proton distance from the center of the H-bond. Thus, α is described as the TS structure $\langle q - Q/2\rangle^{\ddagger}$ relative to the reactant structure $\langle q - Q/2\rangle^{R}$, and scaled by an effective PT distance $\langle q - Q/2\rangle^{P} - \langle q - Q/2\rangle^{R}$. Figure 11a compares eq 4.5 to the electronic structure-based eq 2.6, showing that the behavior is virtually identical. Figure 11b displays the linear geometry−electronic structure correlation between $\langle c_I^2\rangle$ and $\langle q - Q/2\rangle$, discussed in detail in Appendix B.

Given eq 4.5, the Brønsted coefficient slope α_o' is thus related to the relative change in reactant and TS geometric structure with reaction asymmetry (see eq B.6)

$$\alpha_o' = \frac{1}{\langle q - Q/2\rangle^{P} - \langle q - Q/2\rangle^{R}}\left[\frac{\partial\langle q - Q/2\rangle^{\ddagger}}{\partial\Delta G_{RXN}} - \frac{\partial\langle q - Q/2\rangle^{R}}{\partial\Delta G_{RXN}}\right] \tag{4.6}$$

Figure 11c displays the geometric ($\langle q - Q/2\rangle^{\ddagger}$) structure behavior versus ΔG_{RXN} for both H and D, where the structural variation with reaction asymmetry is larger for H than D (see also Figure 6), a variation that correlates with the dependence on the TS ZPE curvature via eqs 2.9 and 2.10.

The remarkable correlation between $\langle c_I^2\rangle$, $\langle q - Q/2\rangle$, and ΔE displayed in Figures 6 and 11c and quantitatively described in Appendix B, together with the Brønsted coefficient in Figure 11a, paints a broad tableau in which TS structure can be characterized: via quantum-averaged geometric structure $\langle q - Q/2\rangle$, quantum-averaged electronic structure $\langle c_I^2\rangle$, or position along the solvent reaction coordinate ΔE.[58]

4c. Analysis of Experimental KIE versus Reaction Asymmetry Behavior and the Marcus Relation. From the adiabatic PT perspective, the numerical analysis of the KIE versus ΔG_{RXN} behavior would naturally involve, and we would advocate, the fit of eq 3.4 to the data, and then interpretation of the parameters. The first of these is the maximum KIE, which gives $\Delta G_{oD}^{\ddagger} - \Delta G_{oH}^{\ddagger}$, interpreted in section 4a.[59] The rate of falloff from the maximum determines the difference in the Brønsted slope α_o', i.e., $\alpha_{oH}' - \alpha_{oD}'$, interpreted in section 4b. Although such an analysis would appear to be straightforward to implement, a different equation is often used to model experimental KIE versus reaction asymmetry data[2], as now discussed.

This alternate analysis is based on the empirical[26] Marcus FER for PT[2c,5,28]

$$\Delta G^{\ddagger} = \Delta G_o^{\ddagger} + \frac{1}{2}\Delta G_{RXN} + \frac{\Delta G_{RXN}^{\ 2}}{16\Delta G_o^{\ddagger}} \tag{4.7}$$

The KIE (H vs D) following from this FER is

$$k_H/k_D = \exp\left[\left(\Delta G_{oD}^{\ddagger} - \Delta G_{oH}^{\ddagger} - \frac{1}{16}\left(\frac{1}{\Delta G_{oH}^{\ddagger}} - \frac{1}{\Delta G_{oD}^{\ddagger}}\right)\Delta G_{RXN}^{\ 2}\right)/RT\right] \tag{4.8}$$

A variant of eq 4.8[2c,5] is often used to model data

$$\ln(k_H/k_D) = \ln(k_{Ho}/k_{Do})\left[1 - \left(\frac{\Delta G_{RXN}^{\ 2}}{16\Delta G_{oH}^{\ddagger}\Delta G_{oD}^{\ddagger}}\right)\right] \approx \ln(k_{Ho}/k_{Do})\left[1 - \left(\frac{\Delta G_{RXN}}{4\Delta G_{oH}^{\ddagger}}\right)^2\right] \tag{4.9}$$

where the second line was derived[2c,5] assuming that $\Delta G_{oH}^{\ddagger} \sim \sqrt{\Delta G_{oH}^{\ddagger}\Delta G_{oD}^{\ddagger}}$. Equation 4.9 allows for an attractive data

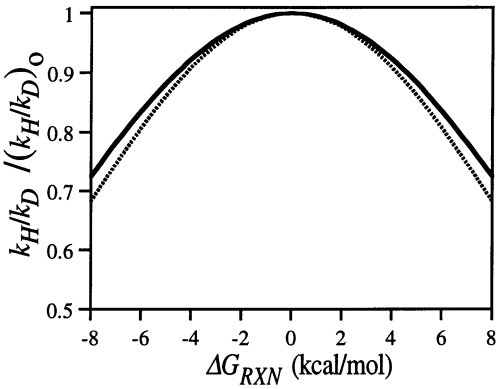

Figure 12. Relative KIE $k_H/k_D/(k_H/k_D)_o$ versus reaction asymmetry for adiabatic PT, eq 3.4 (solid line), and for the Marcus expression, eq 4.10 (dotted line).

analysis, with only two fitting parameters required: the symmetric KIE and the curvature of the KIE falloff.

To make a numerical comparison of the Marcus eq 4.9 with that of adiabatic PT, eq 3.4, we rewrite the former as

$$\frac{k_H}{k_D} = \frac{k_{Ho}}{k_{Do}} \exp\left[-\left(\frac{\Delta G_{RXN}}{4\Delta G^{\ddagger}_{oH}}\right)^2 \ln\left(\frac{k_{Ho}}{k_{Do}}\right)\right] \qquad (4.10)$$

Figure 12 shows the comparison between eq 3.4 and 4.10, where the intrinsic barriers were input parameters to eq 4.10. The difference between the two is small, with only a 15% difference in curvatures. This small difference traces to the small numerical differences in the FERs eqs 4.7 and 2.3, as discussed extensively in section 5d of ref 26a.

Despite this numerical similarity, the attribution of the falloff of the maximum KIE with increased reaction asymmetry to $ZPE^{\ddagger}$ variation, which is common to the standard W−M and adiabatic PT pictures, is not at all explicitly evident in the Marcus KIE expression. This source of the KIE falloff has already been extensively discussed in sections 2b.2 and 3b, and here we only illustrate the point here in the standard perspective.[60] For a general second-order FER for PT of the form eq 2.3, the KIE is given by eq 3.4. In the standard picture, the free energy barrier contains a classical activation energy $\Delta V^{\ddagger}$ for the MEP and a difference in ZPE between reactant and TS (analogous to eq 2.4)

$$\Delta G^{\ddagger} = \Delta V^{\ddagger} + ZPE^{\ddagger} - ZPE^{R} \qquad (4.11)$$

The derivative of α evaluated for the symmetric reaction is thus

$$\alpha'_o = \left.\frac{\partial^2 \Delta G^{\ddagger}}{\partial \Delta G_{RXN}{}^2}\right|_o = \left.\frac{\partial^2 \Delta V^{\ddagger}}{\partial \Delta G_{RXN}{}^2}\right|_o + \left.\frac{\partial^2 (ZPE^{\ddagger} - ZPE^{R})}{\partial \Delta G_{RXN}{}^2}\right|_o \qquad (4.12)$$

Because the first term in eq 4.12 is isotope-independent,[60]

$$\alpha'_{oH} - \alpha'_{oD} = \frac{\partial^2 (ZPE^{\ddagger}_H - ZPE^{R}_H)}{\partial \Delta G_{RXN}{}^2} - \frac{\partial^2 (ZPE^{\ddagger}_D - ZPE^{R}_D)}{\partial \Delta G_{RXN}{}^2} \approx \frac{\partial^2 ZPE^{\ddagger}_H}{\partial \Delta G_{RXN}{}^2} - \frac{\partial^2 ZPE^{\ddagger}_D}{\partial \Delta G_{RXN}{}^2} \qquad (4.13)$$

(which can be compared to the adiabatic PT result eq 2.18). Here the second line follows because the reactant ZPE varies much less than the TS ZPE.[62] Thus, the standard view eq 4.13 quantitatively ascribes the KIE falloff in the standard perspective to the differential rate of TS ZPE change between H and D, a key prediction shared by the adiabatic PT view.

Now, the same approach with the Marcus FER yields

$$\alpha'_{oH} - \alpha'_{oD} = \frac{1}{8(\Delta V^{\ddagger}_o + ZPE^{\ddagger}_{oH} - ZPE^{R}_{oH})} - \frac{1}{8(\Delta V^{\ddagger}_o + ZPE^{\ddagger}_{oD} - ZPE^{R}_{oD})} = \frac{ZPE^{\ddagger}_{oD} - ZPE^{R}_{oD} - ZPE^{R}_{H} - ZPE^{\ddagger}_{oH} + ZPE^{R}_{oH}}{8\Delta G^{\ddagger}_{oH}\Delta G^{\ddagger}_{oD}} \qquad (4.14)$$

in which the falloff is expressed via the difference in magnitude of the $ZPE^{\ddagger}$ for the symmetric reaction, rather than by any variation in $ZPE^{\ddagger}$.[63]

5. Concluding Remarks

A theoretical description of primary KIEs for adiabatic PT reactions has been presented utilizing a nontraditional picture in which the proton nuclear motion is treated quantum mechanically but is not tunneling. This adiabatic PT description strongly differs from the standard treatment of KIEs for PT in both the quantization of the proton and the identification of a solvent coordinate as the reaction coordinate. Four different KIE features observed experimentally, which have been believed to support the standard interpretation of KIEs, have been shown to also follow from this adiabatic PT picture.

However, having emphasized the pronounced differences between the present and standard pictures, it is important to also stress certain general features that the two perspectives share. Namely, a TS theory formalism (see eq 1.2) applies for both pictures in which the KIE exhibits Arrhenius behavior and is primarily determined by the ZPE difference between the reactant and TS for both isotopes. Of course, the definitions of the TS differ considerably in the two pictures: the respective reaction coordinates are entirely different. Further, the mass scaling of ZPEs ($ZPE \propto 1/\sqrt{m}$) allows for similar magnitudes in KIEs and leads to approximate adherence to the Swain−Schaad relationships.

Included in the similarity is the long-held physical organic perspective that the extent of PT in the TS correlates with reaction asymmetry, consistent with the Hammond postulate. For the present adiabatic PT treatment (but not the standard one), the extent of PT at the TS in the solvent coordinate is described (section 4b) in terms of the electronic and geometric structure, averaged over the quantum motion of the proton and H-bond.

A primary difference between the two perspectives concerns the magnitude of the proton ZPE at the TS of a symmetric reaction. In the standard picture, the TS contains no such contribution, whereas the present picture, reflecting the quantum nature of the proton motion, has a finite one (∼1 kcal/mol). This distinct difference, described in section 4a, defines a lower range for the KIE of a symmetric reaction for adiabatic PT than that for the standard picture, consistent with experimental results.

A second key difference between the standard and present approaches is that the reaction coordinate is a solvent coordinate. This shift in perspective focuses attention on the local environment for the PT event and should have important consequences for both solution and enzymatic PT rates.

Acknowledgment. This work was supported in part by NSF grants CHE-9700419 and CHE-0108314. P.K. acknowledges the support of an NIH Postdoctoral Fellowship (4/98-3/00).

Appendix A: α'_o and the Rate of Change of the Transition State ZPE

Here we derive eq 2.18 of the text connecting the Brønsted slope α'_o with variation of ZPEs with reaction asymmetry. The ZPEs in the reactant and TS regions have been quantitatively described by a second-order expansion around their respective critical positions for the symmetric reaction (cf. eqs 5.23 and 5.24 in ref 26a)

$$\mathrm{ZPE}^{\mathrm{R}} = Z^{\mathrm{R}}_{\mathrm{m,o}} - a(\Delta E_{\mathrm{R}} + \Delta E_{\mathrm{o}}) - \frac{b}{2}(\Delta E_{\mathrm{R}} + \Delta E_{\mathrm{o}})^2$$

$$\mathrm{ZPE}^{\ddagger} = Z^{\ddagger}_{\mathrm{m,o}} \mp a^{\ddagger}\Delta E^{\ddagger} - \frac{b^{\ddagger}}{2}\Delta E^{\ddagger 2} \quad \text{(A.1)}$$

where the reactant and TS positions along the reaction coordinate, ΔE_{R} and $\Delta E^{\ddagger}$, respectively, are linearly dependent on the reaction asymmetry

$$\Delta E_{\mathrm{R}} = -\Delta E_{\mathrm{o}} - \frac{\Delta G_{\mathrm{RXN}}}{k_{\mathrm{R}}\Delta\Delta E} \qquad \Delta E^{\ddagger} = \frac{\Delta G_{\mathrm{RXN}}}{k^{\ddagger}\Delta\Delta E} \quad \text{(A.2)}$$

involving the force constants of the free energy for the reactant (k_{R}) and the TS ($k^{\ddagger}$). The $\mp$ in eq A.1 for $\mathrm{ZPE}^{\ddagger}$ ensures that the ZPE is minimal for $\Delta E = 0$ and increases as $|\Delta E|$ increases. The rate of change of the reactant and TS ZPEs with respect to ΔG_{RXN} in the vicinity of the symmetric reaction is thus

$$\frac{\partial \mathrm{ZPE}^{\mathrm{R}}}{\partial \Delta G_{\mathrm{RXN}}} = -a\frac{\partial \Delta E_{\mathrm{R}}}{\partial \Delta G_{\mathrm{RXN}}} \qquad \frac{\partial \mathrm{ZPE}^{\ddagger}}{\partial \Delta G_{\mathrm{RXN}}} = \mp a^{\ddagger}\frac{\partial \Delta E^{\ddagger}}{\partial \Delta G_{\mathrm{RXN}}} \quad \text{(A.3)}$$

The inversely proportional behavior of the derivatives in eq A.2 with the ZPE curvatures k_{R} and $k^{\ddagger}$ demonstrates that the rates of change of the reactant and TS ZPEs in eq A.3 are also inversely related to these curvatures. In particular, because $a^{\ddagger}$ is isotope-independent (a property of the discontinuity at $\Delta E = 0$[26a]), and $\Delta\Delta E$ is relatively isotope-independent, the difference of the H and D rates of $\mathrm{ZPE}^{\ddagger}$ change with reaction asymmetry is solely dependent on the difference in ZPE curvatures at the TS:

$$\left.\frac{\partial \mathrm{ZPE}^{\ddagger}}{\partial \Delta G_{\mathrm{RXN}}}\right|_{\mathrm{oH}} - \left.\frac{\partial \mathrm{ZPE}^{\ddagger}}{\partial \Delta G_{\mathrm{RXN}}}\right|_{\mathrm{oD}} \approx \frac{a^{\ddagger}}{\Delta\Delta E}\left(\frac{1}{k_{\mathrm{H}}{}^{\ddagger}} - \frac{1}{k_{\mathrm{D}}{}^{\ddagger}}\right) \quad \text{(A.4)}$$

To further connect the ZPE curvatures and gradients in eq A.3 with α'_o, we use them to rewrite eq 2.13 as

$$\alpha'_{\mathrm{o}} = \frac{1}{\Delta\Delta E}\frac{\partial(\Delta E^{\ddagger} - \Delta E_{\mathrm{R}})}{\partial \Delta G_{\mathrm{RXN}}} = \frac{1}{\Delta\Delta E}\left[\frac{1}{a^{\ddagger}}\left.\frac{\partial \mathrm{ZPE}^{\ddagger}}{\partial \Delta G_{\mathrm{RXN}}}\right|_{\mathrm{o}} - \frac{1}{a}\frac{\partial \mathrm{ZPE}^{\mathrm{R}}}{\partial \Delta G_{\mathrm{RXN}}}\right] \quad \text{(A.5)}$$

where the gradient of the $\mathrm{ZPE}^{\ddagger}$ is always the positive increase with increasing reaction asymmetry. Note that the two components in eq A.5 exactly correlate with the two terms in eq 2.9. The isotope difference of A.5 is then

$$\alpha'_{\mathrm{oH}} - \alpha'_{\mathrm{oD}} = \frac{1}{\Delta\Delta E}\left[\frac{1}{a^{\ddagger}}\left(\left.\frac{\partial \mathrm{ZPE}^{\ddagger}}{\partial \Delta G_{\mathrm{RXN}}}\right|_{\mathrm{o,H}} - \left.\frac{\partial \mathrm{ZPE}^{\ddagger}}{\partial \Delta G_{\mathrm{RXN}}}\right|_{\mathrm{o,D}}\right) - \left(\frac{1}{a^{\mathrm{H}}}\frac{\partial \mathrm{ZPE}^{\mathrm{R}}_{\mathrm{H}}}{\partial \Delta G_{\mathrm{RXN}}} - \frac{1}{a^{\mathrm{D}}}\frac{\partial \mathrm{ZPE}^{\mathrm{R}}_{\mathrm{D}}}{\partial \Delta G_{\mathrm{RXN}}}\right)\right] \quad \text{(A.6)}$$

and because the first term (72%) dominates the second (28%), the most significant component in $\alpha'_{\mathrm{oH}} - \alpha'_{\mathrm{oD}}$ is proportional to the difference in the rate of increase of the $\mathrm{ZPE}^{\ddagger}$ with increasing reaction asymmetry between H and D.

Appendix B: Correlation between α and Geometric Structure

In this appendix, quantitative relations between geometric structure and α are derived for use in section 4b. We take $\langle q - Q/2\rangle$, the quantum average over both the proton and H-bond coordinates of the proton distance to the center of the H-bond, as a measure of this geometric structure or "extent of PT". $\langle q - Q/2\rangle$ is a function of the solvent coordinate ΔE, a behavior that is isotope-dependent but is independent of reaction asymmetry. This functional property is identical to that for quantum-averaged electronic structure $\langle c_{\mathrm{I}}{}^2\rangle$ and thus, the electronic structure $\langle c_{\mathrm{I}}{}^2\rangle$ uniquely correlates to a geometric structure $\langle q - Q/2\rangle$. This correlation is displayed in Figure 11b, and the apparent linear dependence is represented by

$$\langle c_{\mathrm{I}}{}^2\rangle^c = \frac{1}{2} + \frac{\partial\langle c_{\mathrm{I}}{}^2\rangle}{\partial\langle q - Q/2\rangle}\langle q - Q/2\rangle^c \quad \text{(B.1)}$$

where c represents any critical point (R, P, or ‡). The slope in Figure 11b can physically be described as the ratio of the change in electronic structure between reactant and product ($\langle c_{\mathrm{I}}{}^2\rangle^{\mathrm{P}} - \langle c_{\mathrm{I}}{}^2\rangle^{\mathrm{R}}$) over the effective PT distance ($\langle q - Q/2\rangle^{\mathrm{P}} - \langle q - Q/2\rangle^{\mathrm{R}}$), a value that is isotope-dependent and a physical characteristic of the PT system. Note that eq B.1 can be used to connect $\langle q - Q/2\rangle^{\mathrm{c}}$ to critical points along ΔE,

$$\Delta E^c = \frac{\langle q - Q/2\rangle^c}{k_{\mathrm{d}}}\frac{\partial\langle c_{\mathrm{I}}{}^2\rangle}{\partial\langle q - Q/2\rangle} - \frac{\Delta G_{\mathrm{RXN}}}{k_{\mathrm{d}}\Delta\Delta E} \quad \text{(B.2)}$$

via a relationship between $\langle c_{\mathrm{I}}{}^2\rangle^{\mathrm{c}}$ and ΔE^{c}, similar to that derived previously (cf. eq 5.29 in ref 26a)

$$\Delta E^{\mathrm{c}} = \frac{1}{k_{\mathrm{d}}}\left(\langle c_{\mathrm{I}}{}^2\rangle^{\mathrm{c}} - \frac{1}{2}\right) - \frac{\Delta G_{\mathrm{RXN}}}{k_{\mathrm{d}}\Delta\Delta E} \quad \text{(B.3)}$$

The Brønsted coefficient α is described via eq 2.6 (repeated here) as the relative change in electronic TS structure (or distance along the reaction coordinate)

$$\alpha = \frac{\Delta E^{\ddagger} - \Delta E^{\mathrm{R}}}{\Delta E^{\mathrm{P}} - \Delta E^{\mathrm{R}}} = \frac{\langle c_{\mathrm{I}}{}^2\rangle^{\ddagger} - \langle c_{\mathrm{I}}{}^2\rangle^{\mathrm{R}}}{\langle c_{\mathrm{I}}{}^2\rangle^{\mathrm{P}} - \langle c_{\mathrm{I}}{}^2\rangle^{\mathrm{R}}} \quad \text{(B.4)}$$

Substitution of either eq B.1 or B.2 into eq B.4 yields eq 4.5 of the text:

$$\alpha = \frac{\langle q - Q/2\rangle^{\ddagger} - \langle q - Q/2\rangle^{\mathrm{R}}}{\langle q - Q/2\rangle^{\mathrm{P}} - \langle q - Q/2\rangle^{\mathrm{R}}} \quad \text{(B.5)}$$

The Brønsted coefficient slope α'_o is thus related to the relative change in reactant and TS structures with reaction asymmetry

$$\alpha'_{\mathrm{o}} = \frac{1}{\Delta\Delta q}\left[\frac{\partial\langle q - Q/2\rangle^{\ddagger}}{\partial \Delta G_{\mathrm{RXN}}} - \frac{\partial\langle q - Q/2\rangle^{\mathrm{R}}}{\partial \Delta G_{\mathrm{RXN}}}\right] \quad \text{(B.6)}$$

where $\Delta\Delta q = \langle q - Q/2\rangle^{\mathrm{P}} - \langle q - Q/2\rangle^{\mathrm{R}}$ is a constant for the PT system.

The two terms in eq B.6 directly correlate with the two terms in eq 2.9 of the text, such that variation of TS/reactant structures

with reaction asymmetry is determined by the curvatures in the reactant and TS. The isotopic difference of eq B.6

$$\alpha'_{oH} - \alpha'_{oD} = \left[\frac{1}{\Delta\Delta q_H}\frac{\partial\langle q - Q/2\rangle^{\ddagger}_H}{\partial\Delta G_{RXN}} - \frac{1}{\Delta\Delta q_D}\frac{\partial\langle q - Q/2\rangle^{\ddagger}_D}{\partial\Delta G_{RXN}}\right] - \left[\frac{1}{\Delta\Delta q_H}\frac{\partial\langle q - Q/2\rangle^{R}_H}{\partial\Delta G_{RXN}} - \frac{1}{\Delta\Delta q_D}\frac{\partial\langle q - Q/2\rangle^{R}_D}{\partial\Delta G_{RXN}}\right] \quad \text{(B.7)}$$

is the differential rate of TS−R structural change between H and D, where the first difference measures the isotopic difference in TS structure variation and the second difference measures the isotopic difference in reactant structure variation; the former difference is more quantitatively significant (see section 2b.2).

References and Notes

(1) (a) Bell, R. P. *The Proton in Chemistry*, 2nd ed.; Cornell University Press: Ithaca, NY, 1973. (b) Caldin, E.; Gold, V. *Proton-Transfer Reactions*; Chapman and Hall: London, 1975. (c) Kresge, A. J. *Acc. Chem. Res.* **1975**, *8*, 354. (d) Hibbert, F. *Adv. Phys. Org. Chem.* **1986**, *22*, 113; **1990**, *26*, 255.

(2) (a) Kreevoy, M. M.; Konasewich, D. E. *Adv. Chem. Phys.* **1972**, *21*, 243. (b) Kreevoy, M. M.; Oh, S.-w. *J. Am. Chem. Soc.* **1973**, *95*, 4805. (c) Kresge, A. J.; Silverman, D. N. *Methods Enzymol.* **1999**, *308*, 276. (d) Kresge, A. J.; Chen, H. J.; Chiang, Y. *J. Am. Chem. Soc.* **1977**, *99*, 802. (e) Kresge, A. J.; Sagatys, D. S.; Chen, H. L. *J. Am. Chem. Soc.* **1977**, *99*, 7228. (f) McLennan, D. J.; Wong, R. J. *Aust. J Chem.* **1976**, *29*, 787. (g) Lee, I.-S. H.; Jeoung, E. H.; Kreevoy, M. M. *J. Am. Chem. Soc.* **2001**, *123*, 7492.

(3) (a) Bell, R. P.; Goodall, D. M. *Proc. R. Soc. London Series A* **1966**, *294*, 273. (b) Dixon, J. E.; Bruice, T. C. *J. Am. Chem. Soc.* **1970**, *92*, 905. (c) Pryor, W. A.; Kneipp, K. G. *J. Am. Chem. Soc.* **1971**, *93*, 5584. (d) Bell, R. P.; Cox, B. G. *J. Chem. Soc. B* **1971**, 783. (e) Bordwell, F. G.; Boyle, W. J. *J. Am. Chem. Soc.* **1975**, *97*, 3447.

(4) (a) Kohen, A.; Klinman, J. P. *Acc. Chem. Res.* **1998**, *31*, 397. (b) Kohen, A.; Cannio, R.; Bartolucci, S.; Klinman, J. P. *Nature* **1999**, *399*, 496. (c) Cha, Y.; Murray, C. J.; Klinman, J. P. *Science* **1989**, *243*, 1325.

(5) Kresge, A. J. In *Isotope Effects on Enzyme-Catalyzed Reactions*; Cleland, W. W., O'Leary, M. H., Northrop, D. B., Eds.; University Park Press: Baltimore, MD, 1977, 37.

(6) (a)Westheimer, F. H. *Chem. Rev.* **1961**, *61*, 265. For an earlier review on the topic, see: (b) Melander, L. *Isotope Effects on Reaction Rates*; The Ronald Press Co.: New York, 1960.

(7) Melander, L.; Saunders, W. H. *Reaction Rates of Isotopic Molecules*; Wiley: New York, 1980.

(8) A KIE expression of the form in eq 1.2 neglects any mass dependence in the prefactor, the contribution of which is usually negligible, except in the case of tunneling,[4,7] as well as assumes that the proton primarily resides in it ground (stretching and bending) vibrational state.

(9) (a) Hammond, G. S. *J. Am. Chem. Soc.* **1955**, *77*, 334. (b) Lowry, T. H.; Richardson, K. S. *Mechanism and Theory in Organic Chemistry*, 3rd ed.; Harper Collins Publishers: New York, 1987. (c) Kreevoy[2g] refers to this as the Leffler-Hammond postulate, cf.: Leffler, J. E. *Science* **1953**, *117*, 334.

(10) Swain, G. G.; Stivers, E. C.; Reuwer, J. F.; Schaad, L. J. *J. Am. Chem. Soc.* **1958**, *80*, 5885.

(11) More O'Ferral, R. A. In *Proton-Transfer Reactions*; Caldin, E., Gold, V., Eds.; Chapman and Hall: London, 1975; Chapter 8.

(12) (a) Bell, R. P. *The Tunnel Effect in Chemistry*; Chapman and Hall: NewYork, 1980. (b) Bell, R. P.; Sachs, W. H., Tranter, R. L. *Trans. Faraday Soc.* **1971**, *67*, 1995.

(13) Saunders, W. H. *J. Am. Chem. Soc.* **1985**, *107*, 164.

(14) Kiefer, P. M.; Hynes, J. T. Manuscript in preparation.

(15) For examples of the equilibrium solvation picture for PT in a complex system, see (a) Bash, P. A.; Field, M. J.; Davenport, R. C.; Petsko, G. A.; Ringe, D.; Karplus, M. *Biochemistry* **1991**, *30*, 5826. (b) Cui, Q.; Karplus, M. *J. Am. Chem. Soc.* **2001**, *123*, 2284. (c) Alhambra, C.; Corchado, J.; Sánchez, M. L.; Garcia-Viloca, M.; Gao, J.; Truhlar, D. G. *J. Phys. Chem. B* **2001**, *105*, 11326. (d) Cui, Q.; Elstner, M.; Karplus, M. *J. Phys. Chem. B* **2002**, *106*, 2721.

(16) Calculations of KIEs derived from a classical reaction path (e.g., the MEP) in the presence of a solvent or polar environment typically add quantum corrections to that path.[17] Such a reaction path, however, includes *classical* motion of the proton, especially near the TS, and thus this technique exhibits no difference in quantum corrections between H and D at the TS for a symmetric reaction ($\Delta G_{RXN} = 0$),[17b] in contrast to the present picture. In variational TS theory for gas phase H atom transfer, the TS significantly deviates from the MEP TS and is isotope-dependent.[18] This feature has been calculated for PT in an enzyme, where the KIE has been diminished because the TS position significantly differs between H and D even in a symmetric case.[17e]

(17) (a) Alhambra, C.; Corchado, J. C.; Sánchez, M. L.; Gao, J.; Truhlar, D. G. *J. Am. Chem. Soc.* **2000**, *122*, 8197. (b) Hwang, J.-K.; Warshel, A. *J. Phys. Chem.* **1993**, *97*, 10053. (c) Hwang, J.-K.; Chu, Z. T.; Yadav, A.; Warshel, A. *J. Phys. Chem.* **1991**, *95*, 8445. (d) Hwang, J.-K.; Warshel, A.; *J. Am. Chem. Soc.* **1996**, *118*, 11745. (e) Alhambra, C.; Gao, J.; Corchado, J. C.; Villa, J.; Truhlar, D. G. *J. Am. Chem. Soc.* **1999**, *121*, 2253. (f) Cui, Q.; Karplus, M. *J. Am. Chem. Soc.* **2002**, *124*, 3093.

(18) Garrett, B. C.; Truhlar, D. G. *J. Am. Chem. Soc.* **1979**, *101*, 4534.

(19) (a) Borgis, D.; Hynes, J. T. *J. Phys. Chem.* **1996**, *100*, 1118. (b) Borgis, D.; Hynes, J. T. *Chem. Phys.* **1993**, *170*, 315. (c) Borgis, D.; Lee, S.; Hynes, J. T. *Chem. Phys. Lett.* **1989**, *162*, 19. (d) Lee, S.; Hynes, J. T. *J. Chim. Phys.* **1996**, *93*, 1783.

(20) (a) Dogonadze, R. R.; Kuznetzov, A. M.; Levich, V. G. *Electrochim. Acta* **1968**, *13*, 1025. (b) German, E. D.; Kuznetzov, A. M.; Dogonadze, R. R. *J. Chem. Soc., Faraday Trans. 2* **1980**, *76*, 1128. (c) Kuznetzov, A. M. *Charge Transfer in Physics, Chemistry and Biology: Physical Mechanisms of Elementary Processes and an Introduction to the Theory*; Gordon and Breach Publishers: Amsterdam, 1995. (d) Kuznetzov, A. M.; Ulstrup, J. *Can. J. Chem.* **1999**, *77*, 1085. (e) Sühnel, J.; Gustav, K. *Chem. Phys.* **1984**, *87*, 179.

(21) (a) Ando, K.; Hynes, J. T. *J. Phys. Chem. B* **1997**, *101*, 10464. (b) Ando, K.; Hynes, J. T. *J. Phys. Chem. A* **1999**, *103*, 10398. (c) Staib, A.; Borgis, D.; Hynes, J. T. *J. Chem. Phys.* **1995**, *102*, 2487. (d) Ando, K.; Hynes, J. T, *Adv. Chem. Phys.* **1999**, *110*, 381.

(22) (a) Basilevsky, M. V.; Soudackov, A.; Vener, M. V. *Chem. Phys.* **1995**, *200*, 87. (b) Basilevsky, M. V.; Vener, M. V.; Davidovich, G. V.; Soudackov, A. *Chem. Phys.* **1996**, *208*, 267. (c) Vener, M. V.; Rostov, I. V.; Soudackov, A.; Basilevsky, M. V. *Chem. Phys.* **2000**, *254*, 249.

(23) (a) Agarwal, P. K.; Billeter, S. R.; Hammes-Schiffer, S. *J. Phys. Chem. B* **2002**, *106*, 3283. (b) Agarwal, P. K.; Billeter, S. R.; Rajagopalan, P. T.; Benkovic, S. J., Hammes-Schiffer, S. *Proc. Natl. Acad. Sci. U.S.A.* **2002**, *99*, 2794. (c) Hammes-Schiffer, S. *Chem. Phys. Chem.* **2002**, *3*, 33. (d) Hammes-Schiffer, S.; Billeter, S. R. *Int. Rev. Phys. Chem.* **2001**, *20*, 591. (e) Billeter, S. R.; Webb, S. P.; Agarwal, P. K.; Iordanov, T.; Hammes-Schiffer, S. *J. Am. Chem. Soc.* **2001**, *123*, 11262. (f) Billeter, S. R.; Webb, S. P.; Iordanov, T.; Agarwal, P. K.; Hammes-Schiffer, S. *J. Chem. Phys.* **2001**, *114*, 6925.

(24) Furthermore, acid−base PT in solution involves successive formation of an H-bond, PT within the H-bond complex, and dissociation of the H-bond. H-bond association and dissociation are not discussed within the standard picture, which in this respect coincides with that of gas-phase PT, where the proton ZPE in the reactant is that of an isolated A−H vibration, and the ZPE of that stretch is imagined to be completely lost going to the TS for a symmetric reaction, due to unstable purely proton motion at the TS. H-bond complex formation is known to decrease the A−H stretching frequency, with larger shifts correlated with stronger H-bonds.[25] Thus, for PT within an H-bond complex, a diminished AH stretching frequency should be accounted for.

(25) (a) Novack, A. *Struct. Bonding* **1974**, *18*, 177. (b) Zeegers-Huyskens, T.; Huyskens, P. In *Molecular Interactions*; Ratajcak, H., Orville-Thomas, W. J., Eds.; John Wiley & Sons: New York, 1980; Vol. 2, p. 1.

(26) (a) Kiefer, P. M.; Hynes, J. T. *J. Phys. Chem A* **2002**, *106*, 1834. (b) Kiefer, P. M.; Hynes, J. T. *J. Phys. Chem A* **2002**, *106*, 1850.

(27) For low *T* and a surrounding environment with minimal fluctuation capacity (cf. Limbach, H.-H.; Scherer, G.; Meschede, L.; Aguilar-Parrilla, F.; Wehrle, B.; Braun, J.; Hoelger, C.; Bendict, H.; Buntkowsky, G.; Fehlhammer, W. P.; Elguero, J.; Smith, J. A. S.; Chaudret, B. In *Ultrafast Reaction Dynamics and Solvent Effects*; Gauduel, Y., Rossky, P. J., Eds.; AIP Press: New York, 1994, 225), the standard picture would possibly be a more appropriate description.

(28) (a) Marcus, R. A. *J. Phys. Chem.* **1968**, *72*, 891. (b) Cohen, A. O.; Marcus, R. A. *J. Phys. Chem.* **1968**, *72*, 4249. (c) Marcus, R. A. *J. Am. Chem. Soc.* **1969**, *91*, 7224. (d) Marcus, R. A. *Faraday Symp. Chem. Soc.* **1975**, *10*, 60.

(29) See the discussion in section 2 of ref 26a, where references to the early contributions of Coulson, Mulliken, Bratos, and Warshel will be found.

(30) Timoneda, J. J.; Hynes, J. T. *J. Phys. Chem.* **1991**, *95*, 10431.

(31) For an extensive reference list, see ref 26.

(32) The literature concerning this solvent coordinate for both PT and ET is quite extensive. For examples, see references in ref 26.

(33) Although not pursued within, motion in the solvent coordinate has been explicitly connected to specific molecular rearrangements for HCl[21a] and HF[21b] to water, as well as H_3O^+ to water.[21a]

(34) See, e.g.: (a) Pechukas, P. In *Dynamics of Molecular Collisions, Part B*; Miller, W. H., Ed.; Plenum Press: New York, 1976. (b) Truhlar, D. G.; Garrett, B. C.; Hynes, J. T. *J. Phys. Chem.* **1983**, *87*, 2664. (c) Hynes, J. T. In *Solvent Effects and Chemical Reactivity*; Tapia, O., Bertran, J., Eds.; Kluwer: Amsterdam, 1996; pp 231−258. (d) Truhlar, D. G.; Garrett, B. C.; Klippenstein, S. J. *J. Phys. Chem.* **1996**, *100*, 12771.

(35) Thompson, W.; Hynes, J. T. *J. Phys. Chem. A* **2001**, *105*, 2582.

(36) Gertner, B. J.; Hynes, J. T. *Faraday Discuss.* **1998**, *110*, 301.

(37) (a) Cleland, W. W.; Kreevoy, M. M. *Science* **1994**, *264*, 1887. (b) Cleland, W. W.; Frey, P. A.; Gerlt, J. A. *J. Biol. Chem.* **1998**, *273*, 25529. We stress that in the present work, the "low barrier H-bond" situation occurs at an activated TS configuration in the solvent coordinate.

(38) Kiefer, P. M.; Leite, V. P. B.; Whitnell, R. M. *Chem. Phys.* **1995**, *194*, 33.

(39) Pimentel, G. C.; McClellan, A. L. *The Hydrogen Bond*; W. H. Freeman: New York, 1960.

(40) (a) Steiner, T.; Saenger, W. *Acta Crystallogr.* **1994**, *B50*, 348. (b) Steiner, T. *J. Chem. Soc., Chem. Commun.* **1995**, 1331. (c) Smirnov, S. N.; Benedict, H.; Golubev, N. S.; Denisov, G. S.; Kreevoy, M. M.; Schowen, R. L.; Limbach, H.-H. *Can. J. Chem.* **1999**, *77*, 943. (d) Benedict, H.; Limbach, H.-H.; Wehlan, M.; Fehlhammer, W.-P.; Golubev, N. S.; Janoscheck, R. *J. Am. Chem. Soc.* **1998**, *120*, 2939.

(41) (a) Hynes, J. T. In *The Enzyme Catalysis Process*, NATO ASI Series; Cooper, A., Houben, J. L., Chien, L. C., Eds.; Plenum: New York, 1989; pp 283−292. (b) Hynes, J. T. In *The Theory of Chemical Reaction Dynamics*; Baer, M., Ed.; CRC Press: Boca Raton, FL, 1985; Vol. IV, p. 171. (c) This TST approximation ignores possible reductions of the rate constant associated with recrossing of the barrier in the solvent coordinate. These have been examined via simulation and theory for a model adiabatic PT reaction in ref 21c and found to be rather minor corrections. They might become more significant, however, for very asymmetric reactions where the activation free energy barrier is quite low and broad, and a diffusional description of the solvent coordinate motion might be required. Even in such cases, however, any H/D isotope effect should be mild, entering only via the isotope effect on the equilibrium barrier frequency.

(42) Even for extreme asymmetric reactions where the free energy barrier is close to disappearing, this will occur first for the ground H-bond vibrational state, such that this state remains a good representation for the reaction surface.

(43) ΔG_{RXN} is defined throughout as the free energy difference between reactant and product H-bond complexes, a free energy difference that is rarely experimentally determined. The free energy difference between the solvated protonated and deprotonated forms of the isolated acid and base, i.e., the difference in pK_as, ΔpK_a,[1,2] is related to ΔG_{RXN} simply via work functions to bring the encounter complexes together and to separate them: $2.3RT\Delta pK_a = \Delta G_{RXN} + w_R - w_P$ (cf. refs 2c and 5). This relation can be inserted into the FER eq 2.3 to analyze experimental data. Further, $\Delta G^{\ddagger}$ in eq 2.3 is the reaction barrier between reactant and product H-bond complexes. The reaction barrier for a PT reaction in solution between a separated acid and base, i.e., including the energetic cost w_R of association of the reactant H-bond complex, is $\Delta G^{\ddagger} = w_R + \Delta G_o^{\ddagger} + {}^1/_2(\Delta pK_a - w_R + w_P) + {}^1/_2\alpha_o'(\Delta pK_a - w_R + w_P)^2$.

(44) (a) Evans, M. G.; Polanyi, M. *Trans. Faraday. Soc.* **1936**, *32*, 1340. (b) (b) Evans, M. G.; Polanyi, M. *Trans. Faraday. Soc.* **1938**, *34*, 11. The Evans−Polanyi relations were developed mainly for gas-phase reactions but are also useful in the solution context.

(45) For real systems, α_o is not expected to be exactly 0.5 due to "intrinsic" asymmetry, but the deviation from 0.5 for either H or D is not expected to be significant (cf. ref 42 in ref 26a). Also, the present analysis assumes that the underlying electronic structure variation with PT should be approximately described by two dominant VB structures. This is unlikely to apply to certain PT reactions, most notably those involving carbon acids (cf. ref 42 in ref 26b). Significant deviations from $\alpha_o = 0.5$ have been observed in these cases and those of hydride transfer and excited-state PT, which have been addressed via empirical modifications of the FER form in eq 2.3.[46]

(46) (a) Yates, K. *J. Am. Chem. Soc.* **1986**, *108*, 6511. (b) Kreevoy, M. M.; Lee, I.-S. H. *J. Am. Chem. Soc.* **1984**, *106*, 2550. (c) Lee, I.-S. H.; Jeoung, E. H.; Kreevoy, M. M *J. Am. Chem. Soc.* **1997**, *119*, 2722.

(47) For example, in model calculations we have included the T dependence of the dielectric constant ϵ of water ($T = 0-100$ °C; see: Riddick, J. A.; Bunger, W. B. *Organic Solvents: Physical Properties and Methods of Purification*, 3rd ed.; Wiley-Interscience: New York, 1970; pp 67−68) and find (i) a ∼20% reduction of the rate Arrhenius slopes and (ii) only a slight effect (<5%) on the KIE Arrhenius slope, due to an almost complete cancellation of parallel effects on H and D transfer. However, caution is required for lower polarity systems. For example, model calculations for solvents with ϵ in the range of 20−45 (selected to model experimental systems, i.e.: Shenderovich, I. G.; Burtsev, A. P.; Denisov, G. S.; Golubev, N. S.; Limbach, H. H. *Magn. Reson. Chem.* **2001**, *39*, S91) show that reaction asymmetries (and activation free energies) can be drastically altered, such that even the description of the PT as activated no longer holds. All of the above will be discussed in detail elsewhere.[14]

(48) The A−B equilibrium separation will increase with increasing T due to anharmonicity, which will obviously affect a variety of properties, including reorganization energy, which implies that the intrinsic reaction barrier and KIE will change with T. However, this will not be significant in a relatively small T range.

(49) Antoniou, D.; Schwartz, S. *Proc. Natl. Acad. Sci. U.S.A.* **1997**, *94*, 12360.

(50) In particular, a similar KIE versus ΔG_{RXN} behavior can be observed for the tunneling regime of this new perspective.[14]

(51) Further, any finite reaction asymmetry would likely wipe out such a small reaction barrier.

(52) Personal communication from E. Pines. For preliminary KIEs of photoacids, see: (a) Krishman, R.; Lee, J.; Robinson, G. W. *J. Phys. Chem.* **1990**, *94*, 9635. (b) Pines, E.; Pines, D.; Barak, T.; Magnes, B.-Z.; Tolbert, L. M.; Haubrich, J. E. *Ber. Bunsen-Ges. Phys. Chem.* **1998**, *102*, 511.

(53) The observed KIEs[2c,2e,52] were measured by changing the solvent from H_2O to D_2O, and though this change in solvent introduces other possible solvent isotope effects (i.e., viscosity), the rate-limiting step in each case has been shown to be a PT step (or a series of PT steps), and thus the measured KIE corresponds to PT.

(54) This statement could possibly be used with the standard picture to explain the small symmetric reaction KIE magnitude, presented above, but the plausibility of such a bending vibration has yet to be addressed for the these systems. Furthermore, model calculations by the present authors indicate that the increase in bending frequency would not significantly alter the magnitude of the KIE.

(55) Similar nonadiabatic behavior in which bending motion was explicitly included may be found in ref 23; for the corresponding free energy curves of proton stretch and H-bond vibrational excited states, see ref 35.

(56) We have also carried out a model calculation for a slightly bent H-bond system with an angle of 5° and an A−B H-bond separation $Q =$ 2.7 Å, with reactant and product frequencies $\omega_{stretch} = 2900$ cm^{-1} and $\omega_{bend} = 1400$ cm^{-1}, where the parameters have been chosen to be similar to those of ref 23e. The resulting curves are similar to those of Figure 9b, in that the ground-state reaction is nonadiabatic and bend−stretch mixing must be accounted for in excited state reactions. The former feature is largely caused by the large Q value, with some additional effect arising from the slightly bent geometry.

(57) (a) Johnston, H. S. *Gas-Phase Reaction Rate Theory*; The Ronald Press Co.: New York, 1966. (b) Johnston, H. S.; Parr, C. *J. Am. Chem. Soc.* **1963**, *85*, 2544−2551. (c) Johnston, H. S. *Adv. Chem. Phys.* **1960**, *3*, 131.

(58) As a final technical point, we remark that historically, α has been described in terms of the TS bond order $\alpha = n^{\ddagger}$.[44] However, this was derived for gas-phase reactions, where the bond order in the reactant is zero and unity in the product, which would correspond to infinitely separated acid−base complexes in solution. With this in mind, one could also equivalently write $\alpha = (n^{\ddagger} - n^R)/(n^P - n^R)$, with the TS structure defined in terms of bond order. Hence, α can generally be thought of as an order parameter describing the *relative* TS structure. α_o' is thus the rate of change of the *relative* TS structure with respect to reaction asymmetry.

(59) The deviation in the position of the maximum from $\Delta pK_a = 0$ in a KIE versus ΔpK_a plot will determine $w_R - w_P$ (see ref 43), and thus ΔG_{RXN} as well (e.g., ref 2c).

(60) Here we take the perspective introduced by Johnston[57] for gas-phase H atom transfer, where the TS position is determined by the MEP maximum, and the TS ZPE is evaluated there. Obviously, a variational TS theory approach,[18] where the TS position is determined by the maximum of the MEP plus the transverse ZPE, would dictate different isotopic TS positions, analogous to the procedure of the present perspective (see section 2b.2). However, even in that case, the TS position difference between isotopes will be small except when the TS position significantly deviates from the classical MEP maximum, which is indicative of a predominantly tunneling reaction.[61]

(61) (a) Babamov, V. K.; Marcus, R. A. *J. Chem. Phys.* **1981**, *74*, 1790. (b) Hiller, C.; Manz, J.; Miller, W. H.; Römelt, J. *J. Chem. Phys.* **1983**, *74*, 3850. (c) Miller, W. H. *J. Am. Chem. Soc.* **1979**, *101*, 6819. (d) Skodje, R. T.; Truhlar, D. G.; Garrett, B. C. *J. Chem. Phys.* **1982**, *77*, 5955. (e) Marcus, R. A.; Coltrin, M. E. *J. Chem. Phys.* **1977**, *67*, 2609. (f) Garrett, B. C.; Truhlar, D. G. *J. Chem. Phys.* **1983**, *79*, 4931. (g) Kim, Y.; Kreevoy, M. M. *J. Am. Chem. Soc.* **1992**, *114*, 7116.

(62) This is especially the case for gas-phase H atom transfer where ZPE^R is ΔG_{RXN}-independent.

(63) The Marcus FER for PT was originally presented in the context of gas-phase H atom transfer.[28] As discussed in section 4b, such reactions were traditionally analyzed by finding the maximum along the MEP, i.e., the TS, and then the frequencies parallel and perpendicular to the reaction path were obtained to evaluate the KIE.[57] Often this MEP was described by the bond order n of the bond being formed in a BEBO perspective, with $n^{\ddagger}$ the TS bond order. In this perspective, the reaction free energy barrier is the classical activation energy to the TS plus the ZPE difference between the TS and reactant, corresponding exactly to the KIE in eq 1.2. This analysis, however, precludes the possibility that addition of ZPE to each point along the MEP would change the maximum's position along the profile. (This ZPE variation along the reaction coordinate is analogous to the ZPE variation along the solvent coordinate in Figure 4c, which shifts the position of the TS away from $\Delta E = 0$ for asymmetric reactions.) In fact, when quantum motion perpendicular to the MEP is properly included in the free energy profile for gas phase H atom transfer reactions, the TS significantly deviates from the MEP TS, and this deviation is isotope-

dependent.[18] A FER similar to eq 4.7 was derived by Marcus for the classical MEP, lacking any ZPE contributions, and hence isotope-independent. An isotope dependence was inserted into the FER by adding the TS−reactant ZPE difference to the intrinsic barrier (see ref 24 in ref 28a). This allowed for proper description of the intrinsic barrier for an H atom transfer but did not explicitly describe the change in $ZPE^{\ddagger}$ with reaction asymmetry, an aspect presently in the standard picture. A similar remark applies for α_o'. Further, H/D KIE calculations by the present authors for gas-phase H atom transfer (CH···C → C···HC) using the BEBO perspective[57] versus reaction asymmetry are not well described quantitatively by eq 4.7 when ZPE contributions for either H and D are taken into account.[60] Here the difference in bond energy between the carbon acid and carbon base was varied to give a ΔG_{RXN} range of ±4 kcal/mol. The resulting KIE versus ΔG_{RXN} behavior gave a KIE maximum of 6.8 for the symmetric reaction and dropped to 1.35 for $\Delta G_{RXN} = \pm 4$ kcal/mol, i.e., an 80% drop. For the same ΔG_{RXN} range, using the full Marcus eq 4.8 (with the intrinsic barriers for H and D determined from the previous calculations) gives the exact KIE maximum, but the KIE only drops to 6.7, i.e., by only ∼2%, a very significant disparity.